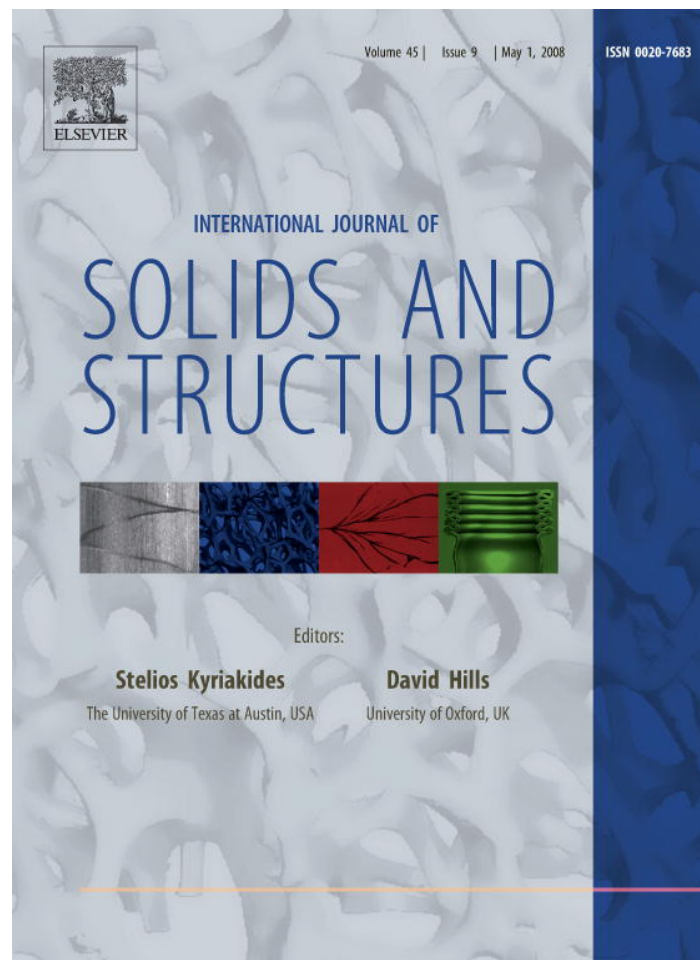


Provided for non-commercial research and education use.  
Not for reproduction, distribution or commercial use.



This article was published in an Elsevier journal. The attached copy is furnished to the author for non-commercial research and education use, including for instruction at the author's institution, sharing with colleagues and providing to institution administration.

Other uses, including reproduction and distribution, or selling or licensing copies, or posting to personal, institutional or third party websites are prohibited.

In most cases authors are permitted to post their version of the article (e.g. in Word or Tex form) to their personal website or institutional repository. Authors requiring further information regarding Elsevier's archiving and manuscript policies are encouraged to visit:

<http://www.elsevier.com/copyright>



# Meso cell model of fiber reinforced composite: Interface stress statistics and debonding paths

V.I. Kushch<sup>a,\*</sup>, S.V. Shmegeera<sup>a</sup>, L. Mishnaevsky Jr.<sup>b</sup>

<sup>a</sup> *Institute for Superhard Materials of the National Academy of Sciences, Composites, 2 Avtozavodskaya Str., 04074 Kiev, Ukraine*

<sup>b</sup> *Risø National Laboratory of the Technical University of Denmark, DK-4000 Roskilde, Denmark*

Received 22 October 2007; received in revised form 22 December 2007

Available online 10 January 2008

---

## Abstract

The primary goal of this work is to develop an efficient analytical tool for the computer simulation of progressive damage in the fiber reinforced composite (FRC) materials and thus to provide the micro mechanics-based theoretical framework for a deeper insight into fatigue phenomena in them. An accurate solution has been obtained for the micro stress field in a meso cell model of fibrous composite. The developed method combines the superposition principle, Kolosov–Muskhelishvili's technique of complex potentials and Fourier series expansion. By using the properly chosen periodic potentials, the primary boundary-value problem stated on the multiple-connected domain has been reduced to an ordinary, well-posed set of linear algebraic equations. The meso cell can include up to several hundred inclusions which is sufficient to account for the micro structure statistics of composite. The presented numerical examples demonstrate an accuracy and high numerical efficiency of the method which makes it to be a promising tool for studying progressive damage in FRCs. By averaging over a number of random structure realizations, the statistically meaningful results have been obtained for both the local stress and effective elastic moduli of disordered fibrous composite. A special attention has been paid to the interface stress statistics and the fiber debonding paths development, which appear to correlate well with the experimental observations.

© 2008 Elsevier Ltd. All rights reserved.

*Keywords:* Fibrous composite material; Cell model; Linear elasticity; Multipole expansion; Interface stress statistics; Debonding path

---

## 1. Introduction

The primary goal of this paper is to develop an efficient tool for the computer simulation of progressive damage in the fiber reinforced composite (FRC) materials and thus to provide the micromechanics-based theoretical framework for a deeper insight into fatigue phenomena in them. Although extensive research in this area has been done during the last decades and a lot of models have been proposed to predict damage accumulation, it should be addressed further attention, in order to meet the challenge of developing models with a more generalized applicability in terms of loading conditions and the materials used. Quoting from Talreja

---

\* Corresponding author. Tel./fax: +380 444329544.

E-mail address: [vkushch@bigmir.net](mailto:vkushch@bigmir.net) (V.I. Kushch).

(2000), “A reliable and cost-effective fatigue life prediction methodology for composite structures requires a physically based modeling of damage evolution. . . A major obstacle to developing mechanistic models for composites is the complexity of the fatigue damage mechanisms, both in their geometry and the details of the evolution process. Overcoming this obstacle requires insightful simplification that allows the use of well-developed mechanics modeling tools without compromising the essential physical nature of the fatigue process”. In the comprehensive review by Degrieck and Van Paepegem (2001), the progressive damage models which use one or more damage variables related to measurable manifestations of damage (interface debonding, transverse matrix cracks, delamination size, etc.) have been claimed as the most promising ones because they quantitatively account for the damage accumulation in the composite structure. The gradual deterioration of a FRC – with a loss of stiffness in the damaged zones – leads to a continuous redistribution of stress and a reduction of stress concentrations inside a structural component (e.g., Allen et al., 1990; Shokrieh and Lessard, 2000; Degrieck and Van Paepegem, 2001). Hence, prediction of the final state of the composite structure requires simulation of the complete path of successive damage states. In order to provide an adequate description of progressive damage with account for the local stress redistribution, one needs to use a complicated structure model, able to reflect both the micro structure statistics and the local damage events. On the other hand, progressive damage simulation implies the boundary-value problem (BVP), stated for this structure model and being a micro mechanical FRC model, to be solved several times. It means that for the problems of this kind the numerical efficiency of solving technique is of critical importance.

The composites of primary interest for us are the unidirectional glass fiber – epoxy matrix FRCs. The prerequisite of using these materials in the wind turbine components is extremely high ( $\sim 10^8$  and more cycles) lifetime. It means that no irreversible strain arise during the loading cycle: in what follows, we restrict our consideration to linear elasticity and transversely loaded unidirectional FRCs. Among a variety of existing FRC models (for a comprehensive review of them, see Buryachenko (2001)), the most advanced are the so-called “multi-particle unit cell” models combining the realistic structure model with an accurate analysis of the relevant BVP, followed by averaging over a series of the random structure realizations. Below, we mention only a few publications utilizing the mentioned approach and most relevant to the topic of a given paper.

In the paper by Babuška et al. (1999), an analysis is focused on the stochastic constitutive properties and statistics of the peak local fiber–matrix interface stresses. For this purpose, a file of the fibers location and their diameter was generated by processing the digitized micrograph of the composite plate cut and these data were used to formulate the structure model and BVP. The traction boundary conditions at the cell sides were taken into account by means of super frame. The numerical method utilized to solve for stress is the  $p$ -version of the finite element method (FEM) combined with the homogenization procedure. Digital image processing technique was used also by Buryachenko et al. (2003) for measurement of centroid coordinates of fibers with the forthcoming estimation of statistical parameters and functions describing the stochastic structure of FRCs. There, the existing algorithms of random micro structures generation have been also reviewed and a comparative statistical analysis of the experimentally measured and numerically simulated fiber distributions has been performed. The approximate multi-particle effective field method (MEFM) is used which allows to estimate the second statistical moments of stresses in both the constituents and the interfaces between the matrix and fibers and thus predict the effective envelope for failure initiation. However, MEFM does not provide evaluation of local stress fields in the constituents and at the interfaces. Chen and Papathanasiou (2004) have used a parallel many-processor implementation of the boundary element method (BEM) to analyze the models containing up to 144 fibers randomly placed inside the square matrix domain. The cell geometry was generated using a Monte Carlo algorithm with controlling the minimum allowable inter-fiber and fiber-cell side spacing. The uniform boundary conditions in displacements and tractions have been applied at the cell sides; the resulting interface stress were found to follow the Weibull-like distribution. Among the many other papers that employ the numerical approach to study random or periodic composites under different conditions at the matrix–fiber interface we also need to mention the FEM-based works by Guedes and Kikuchi (1990), Al-Ostaz and Jasiuk (1996) and Hassini and Hinton (1998), as well as the BEM-based works by Eischen and Torquato (1993), Kaminski (1999), Hu et al. (2000) and Dong (2006).

The known drawbacks of the mentioned above “inclusions inside the box” model are (a) effect of cell boundary on local volume content and arrangement of fibers, (b) uncertainty in formulating the boundary

conditions and (c) stress field distortion near the cell sides. An alternative approach eliminating these undesirable effects consists in using the advanced random packing algorithms (see, e.g., [Torquato, 2002](#)) which provide periodicity of structure at the opposite cell sides and thus enable applying the “natural” periodic boundary conditions. Among the early works following this approach we mention the paper by [Sangani and Yao \(1988\)](#) where the multipole expansion method (MEM) has been applied to reduce the model BVP to an infinite set of linear equations. Noteworthy, MEM is an essentially analytical technique; the numerical effort consists only in evaluating the lattice sums and solving the truncated linear system. Even more numerically efficient version of MEM ([Golovchan et al., 1993](#); [Kushch, 1997](#), among others) utilized the series expansion of displacement vector over a set of appropriate periodic singular solutions. In this case, the matrix coefficients are expressed in terms of the easy-to-calculate sums and the only remaining problem is to find an efficient way to solve the resulting set of linear equations.

Among the other analytical approach-based publications in the area, we mention the paper by [Linkov and Koshelev \(1999\)](#) and book [Linkov \(2002\)](#) utilizing the integral representation for the periodic and double periodic potentials and the works by [Helsing \(1995\)](#), [Cohen and Bergman \(2003\)](#) and [Bonnet \(2007\)](#), where the various series expansions of the displacement field were employed. The superposition principle, Kolosov–Muskhelishvili’s technique of complex potentials and Fourier series expansion were applied by [Mogilevskaya and Crouch \(2001\)](#), [Mogilevskaya and Crouch \(2002\)](#), [Mogilevskaya and Crouch \(2004\)](#) and by [Wang et al. \(2005a,b, 2006\)](#) to reduce the model BVP to an ordinary set of linear algebraic equations. So, in the paper by [Wang et al. \(2005a\)](#), a composite material is modeled by a finite rectangular domain containing multiple circular elastic inclusions and embedded within a larger circular domain with fictitious boundary loading represented by truncated Fourier series. The analytical solution for the complementary problem of a circular domain containing holes and inclusions is obtained by using a combination of the series expansion technique with a direct boundary integral method. This approach is advantageous in that all the integrals are evaluated analytically and the elastic fields and effective properties are expressed explicitly in terms of the coefficients in the series expansions. It makes the numerical algorithm more efficient in comparison with the purely numerical FEM and BEM schemes.

Recently, the very efficient solving techniques have been developed based the fast multipole method ([Greengard, 1994](#); [Sangani and Mo, 1996](#); [Kushch et al., 2002](#); [Wang et al., 2005b](#), among others). In this and similar advanced though rather involved algorithms, a computational effort scales as  $O(N)$ , where  $N$  is a number of inclusions per cell, which makes it rather efficient for studying the very large models (say, with  $N = 1000$  and more), often used in the fluid suspension mechanics in order to account for the long-range interactions accurately. In the solid composites no such long-range interactions exist, and a number from 100 and 200 fibers per cell was reported by many authors as quite sufficient to provide the statistically meaningful results.

Why do we need to seek for the numerically efficient method? An answer given already at the beginning of this paper is the progressive damage models we aim to built up. In these models, in order to simulate the complete path of successive damage, one must solve the model BVP repeatedly several tens or even hundreds times. As the literature review and our analysis shows, neither FEM nor BEM allow to do it with a non-prohibitive computational effort.

In the present work, an analytical approach by [Golovchan et al. \(1993\)](#) has been further developed and applied for studying the local stress and the effective elastic properties of FRC composite using the meso cell model. The paper is organized as follows. In the first section, a choice of the geometry model is substantiated and the problem statement have been given. In the second section, the theory of method and the analytical technique have been derived. It is shown, in particular, that the developed method is sufficiently flexible to consider the both “composite bulk” and “composite ply” models with an adequate account for the edge effects. Next, the details of numerical implementation and the possible ways of improving the numerical efficiency are discussed. The numerical results presented in this section demonstrate the convergence rate of solution, the inter-fiber distance effect and the statistics of interface stress concentration obtained from a series of large-scale numerical experiments. Also, the damage patterns in the form of debonded fiber chains were simulated using a simple debonding model and the results were found to be in agreement with those observed experimentally. Finally, [Appendix A](#) contains the necessary theoretical derivations.

## 2. The model problem statement

### 2.1. Model geometry

The many-inclusion 2D unit cell model of the FRC bulk, shown in Fig. 1, represents the next step in development of the “finite array of inclusions” model studied by Kushch et al. (2005) and Buryachenko and Kushch (2006). Namely, we consider a quasi-random, or generalized periodic, model structure (Golovchan et al., 1993; Bystroem, 2003, among others) with the periods  $a$  and  $b$  along the axes  $Ox_1$  and  $Ox_2$ , respectively, a unit cell of which contains a certain number of aligned in  $x_3$  direction and circular in cross-section fibers. Within such a cell, the fibers can be placed arbitrarily but without overlapping. The fibers whose edges are shown in Fig. 1 by dashed line do not belong to the cell while occupying a certain area within it. Thus, geometry of the unit cell is given by its length  $a$  and height  $b$ , the coordinates  $(X_{1q}, X_{2q})$  being the centers of inclusions  $O_q$  and their radii  $R_q, q = 1, 2, \dots, N$ . The whole composite bulk can be obtained by translating the cell in two orthogonal directions. Besides the global Cartesian coordinate system  $Ox_1x_2$ , we introduce the local, inclusion-related coordinate systems  $Ox_{1q}x_{2q}$  with origins in  $O_q$ . Also, we will use the following complex-valued variables

$$z = x_1 + ix_2, \quad z_q = x_{1q} + ix_{2q}; \tag{1}$$

representing the point  $\mathbf{x} = (x_1, x_2)^T$  in the complex planes  $Ox_1x_2$  and  $Ox_{1q}x_{2q}$ , respectively. Clearly,  $z = z_q + Z_q$ , where  $Z_q = X_{1q} + iX_{2q}$ . Number  $N$  of the fibers with centers inside the cell can be taken large sufficiently to simulate micro structure of an actual disordered composite. In the considered model, a diameter and the elastic moduli are defined individually for each separate fiber. It provides applicability of this model for studying the multi-component systems and the effect of fiber diameter scattering, which can be quite considerable even in the commercial FRCs, see Babuška et al. (1999).

To generate the quasi-random structure shown in Fig. 1, the 2D version of the molecular dynamics (MD) algorithm (for the details, see Sangani and Yao, 1988) of growing particles is utilized. An idea of the algorithm is as follows: we start with a certain prescribed number of tiny fibers whose initial positions within a cell and initial velocities are given by the random number generator. Then, the fibers move toward each other, collide elastically and grow steadily during a period of  $1000N$  collisions. In the case any fiber (more exactly, its center) traversed the cell boundary, it enters the cell from the opposite side. It preserves both the fiber volume content and periodicity of structure. After the volume content of fibers reached the prescribed value, the system is

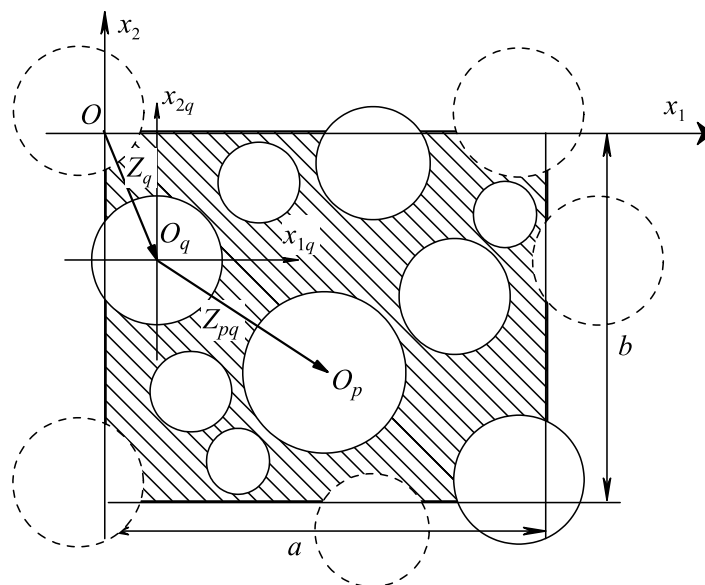


Fig. 1. Structure model of the composite bulk.

further equilibrated for a period of 5000N collisions, sufficient to guarantee reproducible thermodynamic properties of the model (Torquato, 2002).

The considered geometry can be characterized by several parameters, such as packing density, coordination number, radial distribution function (RDF), inter-fiber spacing, etc. In Fig. 2, the empirical RDF for the model FRC with  $N = 100$  and volume content of fibers  $c = 0.65$  is shown. The open circles represent data for a single structure realization, solid circles are obtained by averaging over 10 runs. The solid and dash-dotted lines show the analogous data obtained by Truskett et al. (1998) and Buryachenko et al. (2003), respectively; as seen from the plot, our data practically coincide with the results by Truskett et al. (1998). And yet another parameter often introduced in the many-fiber models of FRC is the “minimum allowable inter-fiber spacing”  $\delta_{\min} = \min_{p,q} (|Z_{pq}|/D - 1)$  (e.g., Chen and Papathanasiou, 2004), where  $D$  is a diameter of fiber and  $Z_{pq} = Z_p - Z_q$ , see Fig. 1. It is usually assigned some small positive value in order to separate inclusions and thus alleviate either analytical or numerical analysis of the model BVP.

The following modification of the above model is also of practical interest. In Fig. 3a, a typical structure of cross-ply FRC laminate is shown: applicability of the composite bulk meso cell model (Fig. 1) does not seem obvious in this case. Say, Babuška et al. (1999) have reported considerable (up to 20%) local decrease of the fiber volume content in the vicinity of inter-ply boundary. Expectably, the stress field in this area will be substantially different of that in the bulk resulting in such damage mode as delamination. Probably, the more adequate model of composite ply is shown in Fig. 4: the only difference from the “bulk model” consists in that no fiber intersections with the flat edges  $x_1 = 0$  and  $x_2 = -b$  of the ply are allowed. The minor modification of the relevant MD algorithm reduces to the assumption that the moving fibers rebound elastically from the ply boundaries instead of penetrating them. This model makes possible studying the edge effects caused by the low fiber volume content nearby the ply boundary and by interacting with the neighboring plies provided the boundary conditions flat edges were properly stated. Under assumption that the boundary conditions at the flat edges of ply are periodic in  $x_1$  with period  $a$  (constants, as a particular case), the stress field will be periodic in  $x_1$  as well. It allows to (a) reformulate the primary “composite bulk” or “composite ply” problem as the BVP for a piece-homogeneous finite-sized cell and (b) confine finding the solution of relevant BVP to the class of periodic functions. It will be seen from the subsequent account that the method we develop can be applied equally to both these models.

Noteworthy, the model we consider involves the additional structure parameter, namely ply thickness  $b \gg R_q$ , so it can be thought as a meso level model. Also, it seems reasonable to regard the typical damage observed in Fig. 3b as the meso level event rather than micro- or macroscopic ones, commonly associated with

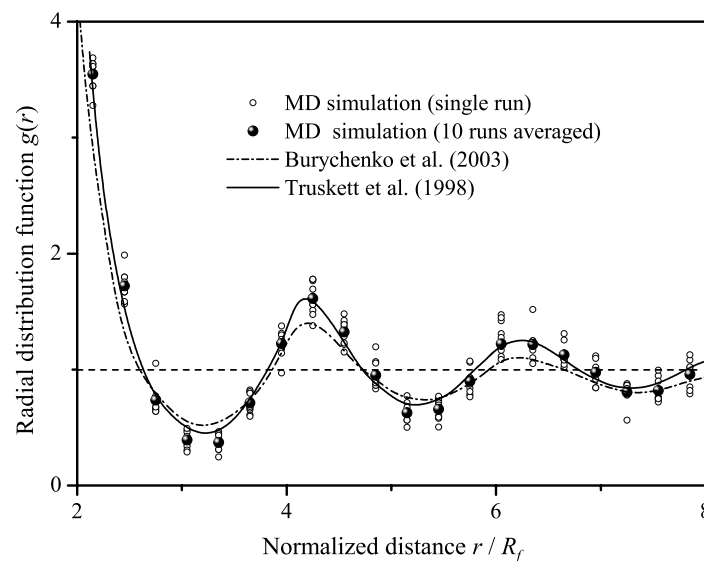


Fig. 2. Radial distribution function of the quasi-random composite cell model: 100 fibers per cell, solid line is obtained by averaging over 10 realizations.

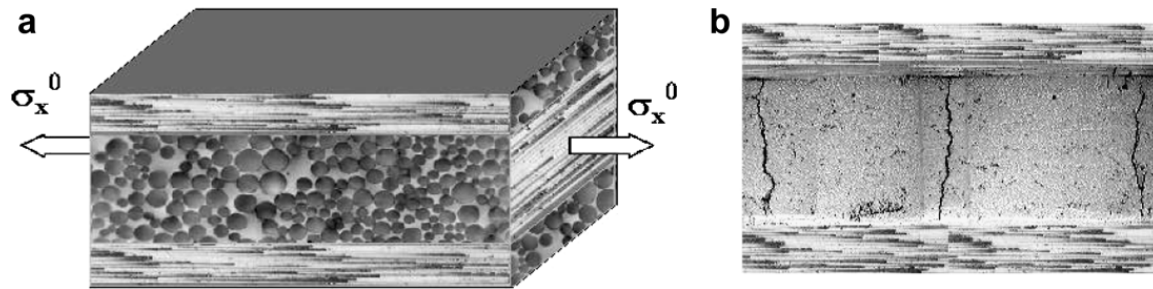


Fig. 3. Cross-ply laminate (a) subjected to uniaxial loading and (b) resulting damage (Joffe, 1999). The figure is reproduced with kind permission from the author.

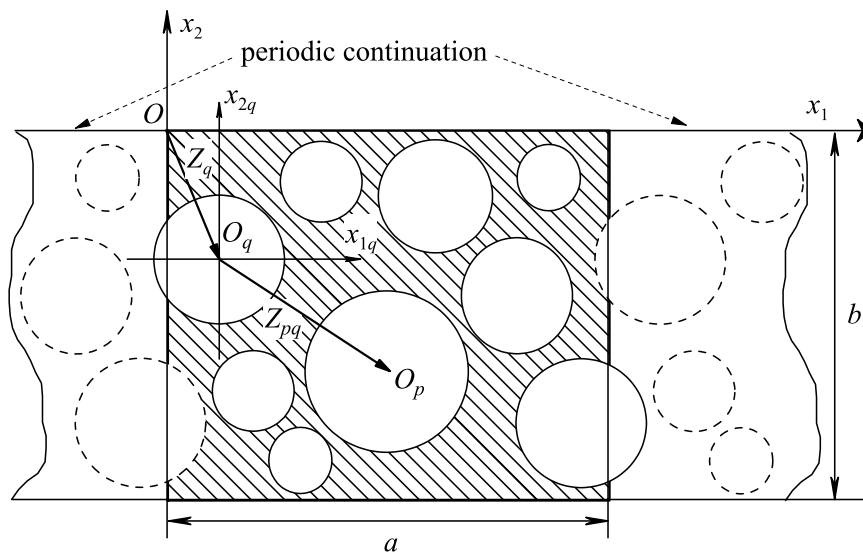


Fig. 4. Structure model of the composite ply.

a single fiber and entire composite part, respectively. Due to these reasons, we will call our model as a “meso cell”; for more discussion on the subject, see Mishnaevsky (2007).

### 2.2. Model problem

By adopting 2D model, we assume implicitly  $\partial\sigma_{ij}/\partial x_3 = 0$ : within this framework, the (a) plane strain, (b) plane stress and (c) anti-plane shear (in  $x_3$ -direction) problems can be studied. Specifically, we consider the plane strain problem ( $u_3 = 0$ ); as a consequence,  $\epsilon_{33} = \epsilon_{13} = \epsilon_{23} = 0$  as well. Both the matrix and fiber materials are isotropic and linearly elastic.

We denote  $u_m = u_{m1} + iu_{m2}$  the displacement in a matrix material with a shear modulus  $G_0$  and Poisson ratio  $\nu_0$ ;  $u_i^{(q)}$ ,  $G_q$  and  $\nu_q$  refer to displacement and elastic moduli, respectively, of  $q$ th fiber,  $q = 1, 2, \dots, N$ . Here,  $u_i$  are the Cartesian components of displacement vector  $\mathbf{u} = (u_1, u_2)^T$ . At the matrix–fiber interfaces, the perfect bonding conditions are prescribed:

$$(u_m - u_i^{(q)})|_{r_q=R_q} = 0; \quad [\tau_n(u_m) - \tau_n(u_i^{(q)})]|_{r_q=R_q} = 0; \quad q = 1, 2, \dots, N; \quad (2)$$

where  $\tau_n = \sigma_{rr} + i\sigma_{r\phi}$ .

The stress field in the composite bulk is assumed to be macroscopically homogeneous, which means constancy of the volume-averaged, or macroscopic, strain  $\mathbf{E} = \{E_{ij}\} = \{\langle\epsilon_{ij}\rangle\}$  and stress  $\mathbf{S} = \{S_{ij}\} = \{\langle\sigma_{ij}\rangle\}$  tensors, where  $V \langle f \rangle = \int_V f dV$  and  $V$  is the volume of meso cell. Sometimes (e.g., Drago and Pindera, 2007), the last one is called as a representative unit cell (RUC) in contrast to the representative volume element (RVE),

which characterizes heterogenous materials with statistically homogeneous microstructures at an appropriate scale. For more discussion regarding the RUC and RVE concepts, their proper choice and the statements of model BVPs, see Shen and Brinson (2006), Drugan and Willis (1996), Gusev (1997), among others. We mention only that for the considered model and the problem under study, namely, statistically homogeneous composite structure and macroscopically homogeneous stress field, they are equivalent in the sense that averaging over RUC and RVE gives the same result provided the last one is taken sufficiently large.

In the problem we consider, the far field load is defined by the macroscopic strain tensor  $\mathbf{E}$ . This statement is typical in the homogenization problem where the macroscopic, or effective, moduli are to be determined. On the contrary, using the macroscopic stress tensor  $\mathbf{S}$  as the load governing parameter is preferable in the local stress concentration study. For this purpose, the established below simple relationships (64) (Section 3.4) can be utilized. Next, it is of common knowledge that under macroscopic stress homogeneity condition periodicity of structure results in periodicity of relevant physical fields. In our case, the periodicity condition

$$\sigma_{ij}(z + a) = \sigma_{ij}(z + ib) = \sigma_{ij}(z) \tag{3}$$

can be alternatively regarded as the cell boundary condition providing continuity of the displacement and stress fields between the adjacent cells. The stress field in the composite ply is governed by a self-equilibrated set of load applied to the flat boundaries and, in the case the boundary conditions at the ply edges are periodic in  $x_1$  with period  $a$  (constants, as a particular case), the stress field will be periodic in  $x_1$  as well:

$$\sigma_{ij}(z + a) = \sigma_{ij}(z). \tag{4}$$

In both the cases, it is possible to decompose the displacement field into a sum of the linear part  $u_0$  being the far field and determined entirely by the  $\mathbf{E}$  tensor and the periodic fluctuation  $u_f$  caused by the inhomogeneities.

The theory we apply to study this problem is the Kolosov–Muskhelishvili’s method of complex potentials, widely recognized as the powerful analytical technique for a given class of problems. However, unlike the case of a finite array of inclusions (Buryachenko and Kushch, 2006; Mogilevskaya and Crouch, 2001), periodicity of the model implies introducing the appropriate periodic complex potentials. The computational cost-efficient way to build up solution of the model BVP in the class of periodic (rather than doubly periodic) functions has been suggested by Golovchan et al. (1993); a brief summary of the theory of periodic potentials is given in Appendix A.

### 3. The problem solution

#### 3.1. Composite band

First, we solve for stress in a “composite band” obtained by removing upper and bottom edges of ply or, equivalently, by putting  $b = \infty$ . In fact, we study a plane containing several periodic rows of circular inclusions. We focus on this auxiliary problem mainly to demonstrate the technique of reducing the boundary-value problem to a linear set of algebraic equations. Then, a composite space and a finite thickness composite ply will be considered in the same manner, with the relevant boundary conditions at the flat edges additionally applied.

We will use the following representation of complex-value displacement

$$u = u_1 + iu_2 = \kappa\varphi(z) - (z - \bar{z})\overline{\varphi'(z)} - \overline{\psi(z)}, \tag{5}$$

slightly different in form but equivalent to that suggested in the original book by Muskhelishvili (1953). In (5), the functions  $\varphi(z)$  and  $\psi(z)$  are the complex potentials,  $\kappa$  is the constant factor equal to  $3 - 4\nu$  for the plane strain problem and  $\bar{z}$  means the complex conjugate of  $z$ . As we will see later on, presence of the multiplier  $(z - \bar{z}) = 2ix_2$  instead of  $z$  in the bi-harmonic term simplifies considerably the solving procedure. Namely, it enables using the periodic potentials in exactly the same way we worked with the conventional potentials of  $z^n$  type in the “finite array of inclusion” problem. Corresponding to (5) the stress tensor is given by

$$\begin{aligned} \sigma_{11} + \sigma_{22} &= 4G_0(\varphi'(z) + \overline{\varphi'(z)}); \\ \sigma_{22} - \sigma_{11} + 2i\sigma_{12} &= 4G_0[(\bar{z} - z)\varphi''(z) - \varphi'(z) + \psi'(z)]. \end{aligned} \tag{6}$$

Following Buryachenko and Kushch (2006), we write a general solution for the plane containing a *finite* row of circular inclusions with centers  $Z_k = ak, |k| \leq K$  as a superposition of the far displacement field  $u_0$  and the disturbances induced by each separate inclusion:

$$u_m = u_0(z) + \sum_{k=-K}^K [\kappa_0 \varphi_k(z_k) - (z_k - \bar{z}_k) \overline{\varphi'_k(z_k)} - \overline{\psi_k(z_k)}], \quad (7)$$

where

$$\varphi_k(z_k) = \sum_{n=1}^{\infty} \frac{a_n^{(k)}}{(z_k)^n}, \quad \psi_k(z_k) = \sum_{n=1}^{\infty} \frac{b_n^{(k)}}{(z_k)^n}, \quad (8)$$

and  $z_k = z - Z_k$ . Note, that in this specific case  $(z_k - \bar{z}_k)$  is independent of index  $k$  and, thus, (7) can be rewritten in the form (5), with the potentials

$$\varphi_{\Sigma}(z) = \sum_{k=-K}^K \varphi_k(z_k); \quad \psi_{\Sigma}(z) = \sum_{k=-K}^K \psi_k(z_k). \quad (9)$$

Now, we recognize that solution for a plane with an *infinite* row on inclusions can be thought as a limiting case of (7)–(9) where  $K \rightarrow \infty$ . Moreover, periodicity of solution implies  $a_n^{(k)} = a_n$  and  $b_n^{(k)} = b_n$  for any  $k$ . As easy to see, by change of summation order in (8) and (9) we come again to solution in the form (5), with the periodic potentials  $t_n(z)$  (A.1):

$$\varphi(z) = \sum_{n=1}^{\infty} a_n t_n(z) \quad \text{and} \quad \psi(z) = \sum_{n=1}^{\infty} b_n t_n(z). \quad (10)$$

Quite analogous consideration shows also that for a more general model involving several, say  $N$ , infinite rows of fibers a general solution will be

$$u_m = u_0(z) + \sum_{p=1}^N u_{ps}(z_p), \quad (11)$$

where

$$u_{ps}(z_p) = \kappa_0 \varphi_{ps}(z_p) - (z_p - \bar{z}_p) \overline{\varphi'_{ps}(z_p)} - \overline{\psi_{ps}(z_p)} \quad (12)$$

and

$$\varphi_{ps}(z_p) = \sum_{n=1}^{\infty} a_n^{(p)} t_n(z_p), \quad \psi_{ps}(z_p) = \sum_{n=1}^{\infty} b_n^{(p)} t_n(z_p). \quad (13)$$

In (13),  $a_n^{(p)}$  and  $b_n^{(p)}$  are the unknown complex-valued coefficients. To be consistent with the above made macroscopic homogeneity assumption, the far displacement field  $u_0$  must be linear:

$$u_0(z) = \Gamma_0 + (\kappa_0 - 1)\Gamma_1 z - (\bar{\Gamma}_2 - \Gamma_1)\bar{z}. \quad (14)$$

Two governing parameters,  $\Gamma_1$  and  $\Gamma_2$ , relate the far field strains  $E_{ij}$  in a way defined below (Eq. (58)); for a while, we consider them as the arbitrary complex constants.

With the potentials taken in the form (10), the periodicity condition (4) is fulfilled automatically. Moreover, due to periodicity of the solution, it suffices to satisfy the interface conditions (2) for the fibers with centers lying inside the unit cell only. We write displacement in  $q$ th fiber as

$$u_i^{(q)} = \kappa_q \varphi_{qr}(z_q) - (z_q - \bar{z}_q) \overline{\varphi'_{qr}(z_q)} - \overline{\psi_{qr}(z_q)}, \quad (15)$$

where the potentials

$$\varphi_{qr}(z_q) = \sum_{n=0}^{\infty} c_{-n}^{(q)}(z_q)^n, \quad \psi_{qr}(z_q) = \sum_{n=0}^{\infty} d_{-n}^{(q)}(z_q)^n \quad (16)$$

are the regular analytical functions.

Noteworthy,  $u_i^{(q)}$  are written in the local coordinates of  $q$ th fiber. To fulfill the conditions (2), one has first to find the local expansion of  $u_m$  in a vicinity of  $O_q$  as well. For  $u_0$ , such an expansion is straightforward:

$$u_0 = U_{0q} + R_q[(\kappa_0 - 1)\Gamma_1 \exp(i\phi_q) - (\overline{\Gamma_2} - \Gamma_1) \exp(-i\phi_q)], \tag{17}$$

where  $z_q = r_q e^{i\phi_q}$  and

$$U_{0q} = \Gamma_0 + (\kappa_0 - 1)\Gamma_1 Z_q - (\overline{\Gamma_2} - \Gamma_1)\overline{Z}_q. \tag{18}$$

Transformation of  $u_{ps}(z_p)$  (12) is based on the formulas (A.4)–(A.7) of Appendix A; taking account of  $z_p = z_q - Z_{pq}$ , we get

$$\sum_{p=1}^N \varphi_{ps}(z_p) = \sum_{p=1}^N \sum_{n=1}^{\infty} a_n^{(p)} t_n(z_p) = \sum_{p=1}^N \sum_{n=1}^{\infty} a_n^{(p)} \left[ \frac{\delta_{pq}}{(z_q)^n} + \sum_{m=0}^{\infty} H_{nm}^*(Z_{pq})(z_q)^m \right] = \sum_n a_n^{(q)} (z_q)^{-n}; \tag{19}$$

where

$$a_{-n}^{(q)} = \sum_{p=1}^N \sum_{m=1}^{\infty} a_m^{(p)} H_{mn}^*(Z_{pq}), \quad n = 0, 1, 2, \dots \tag{20}$$

Applying the same procedure to the rest of terms in (11) and (12) gives us, after some algebra, the following local expansion:

$$u_m = \kappa_0 \sum_n a_n^{(q)} (z_q)^{-n} - (z_q - \overline{z}_q) \sum_n (-n) \overline{a_n^{(q)}} (\overline{z}_q)^{-n-1} - \sum_n \overline{b_n^{(q)}} (\overline{z}_q)^{-n}, \tag{21}$$

where

$$b_{-n}^{(q)} = \sum_{p=1}^N \sum_{m=1}^{\infty} [b_m^{(p)} H_{mn}^*(Z_{pq}) + (n+1)(\overline{Z}_{pq} - Z_{pq}) a_m^{(p)} H_{m,n+1}^*(Z_{pq})], \tag{22}$$

$$n = 0, 1, 2, \dots$$

The last step is substitution of (21) together with (15) into the first of interface conditions (2) and equating to zero the coefficients of the power series in  $z_q$  in the left hand side of (2). As a result, we obtain an infinite set of linear algebraic equations with the unknowns  $a_n^{(p)}$ ,  $b_n^{(p)}$ ,  $c_n^{(p)}$  and  $d_n^{(p)}$ . This procedure resembles closely that one described by Buryachenko and Kushch (2006) and we do not reproduce it here. The second set of equations is born by the second of interface conditions (2) where the curvilinear components of  $\tau_n$  are expressed in terms of complex potentials by the formula

$$(\sigma_r - i\sigma_{r\phi}) = \frac{1}{2} [\sigma_{11} + \sigma_{22} - (\sigma_{22} - \sigma_{11} + 2i\sigma_{12})e^{2i\phi}] = 2G\{2\text{Re}[\varphi'(z)] - [\overline{z}\varphi''(z) + \psi'(z)]e^{2i\phi}\}. \tag{23}$$

The final form of linear algebraic system, obtained after excluding the unknowns  $c_n^{(p)}$  and  $d_n^{(p)}$ , is

$$\frac{\Omega_1}{(R_q)^{2k}} [(R_q)^2(k-2)a_{k-2}^{(q)} - (b_k^{(q)} + ka_k^{(q)})] + \overline{a_{-k}^{(q)}} = -\delta_{k1}\Gamma_1;$$

$$\frac{\Omega_2}{(R_q)^{2k}} a_k^{(q)} - (k+2)(R_q)^2 \overline{a_{-k-2}^{(q)}} - (\overline{b_{-k}^{(q)}} - ka_{-k}^{(q)}) = \delta_{k1}(\overline{\Gamma_2} - \Gamma_1);$$

$$q = 1, 2, \dots, N; \quad k = 1, 2, \dots;$$

where

$$\Omega_1 = \frac{(2\tilde{G}_q + \kappa_q - 1)}{2[\tilde{G}_q(\kappa_0 - 1) + (\kappa_q - 1)]} \text{ for } k = 1, \quad \Omega_1 = \frac{(\tilde{G}_q + \kappa_q)}{2(\tilde{G}_q\kappa_0 - \kappa_q)} \text{ for } k > 1 \tag{25}$$

and

$$\Omega_2 = \frac{(\tilde{G}_q \kappa_0 + 1)}{2(\tilde{G}_q - 1)}; \quad \tilde{G}_q = G_q/G_0.$$

Eq. (24) together with (21) and (21) form a closed infinite well-posed set of linear equations. Based on the results by Golovchan et al. (1993), it is rather straightforward to show that this system belongs to the class of systems with the normal type determinant and thus its solution can be obtained by the truncation method (Kantorovich and Krylov, 1964). After we have  $a_n^{(p)}$  and  $b_n^{(p)}$  found from (24), the coefficients  $c_n^{(p)}$  and  $d_n^{(p)}$  are calculated according to

$$\begin{aligned} c_{-k}^{(q)} &= \frac{(\kappa_0 + 1)}{(\tilde{G}_q + \kappa_q)} a_k^{(q)}, \quad k > 1; \\ \operatorname{Re} c_{-1}^{(q)} &= \frac{(\kappa_0 + 1)}{(2\tilde{G}_q + \kappa_q - 1)} \operatorname{Re}(a_1^{(q)} + \Gamma_1); \\ \operatorname{Im} c_{-1}^{(q)} &= \frac{(\kappa_0 + 1)}{(\kappa_q + 1)} \operatorname{Im}(a_1^{(q)}); \\ d_{-k}^{(q)} &= kc_{-k}^{(q)} + \frac{(\kappa_0 + 1)}{(\tilde{G}_q - 1)} \frac{\overline{a_k^{(q)}}}{(R_q)^{2k}} - (R_q)^2(k + 2)c_{-(k+2)}^{(q)}, \quad k \geq 1; \\ d_0^{(q)} &= 2(R_q)^2(a_{-2}^{(q)} - c_{-2}^{(q)}) + b_0^{(q)} + \overline{B_0^{(q)}} - \kappa_0 \overline{a_0^{(q)}} - (\kappa_0 - 1)\Gamma_1 Z_q + (\overline{\Gamma_2} - \Gamma_1)\overline{Z}_q - U_{0q}; \end{aligned} \tag{26}$$

and, thus, the solution has been completed.

It is appropriate to emphasize here that the exposed solving procedure utilizing the superposition of singular solutions and their local re-expansion in terms of regular ones is the nothing else but the basic multipole expansion technique and thus our approach can be viewed as one of possible realizations of the MEM.

### 3.2. Quasi-random composite space

Now, we come back to the problem stated in the Section 1 (Fig. 1) and show how to satisfy the periodicity conditions (3) in  $x_2$  direction, namely

$$T_n(z - bi) = T_n(z), \quad \text{where } T_n = \sigma_{22} + i\sigma_{12}. \tag{27}$$

For this purpose, we introduce the potentials

$$\varphi_h(z) = \sum_{m \neq 0} p_m \exp(i\beta_m z), \quad \psi_h(z) = \sum_{m \neq 0} q_m \exp(i\beta_m z), \quad \beta_m = 2\pi m/a; \tag{28}$$

written in global variables. In accordance with the superposition principle, a general solution in the matrix domain  $u_m$  (11) takes the form

$$u_m = u_0(z) + \sum_{p=1}^N u_{ps}(z_p) + u_h(z), \tag{29}$$

where  $u_h$  is the boundary-related term, which by analogy with (5) can be expressed as

$$u_h = \kappa_0 \varphi_h(z) - (z - \bar{z})\overline{\varphi'_h(z)} - \overline{\psi_h(z)} = \sum_{m \neq 0} \{ \kappa_0 p_m \exp(i\beta_m z) + [(z - \bar{z})i\beta_m \overline{p_m} - \overline{q_m}] \exp(-i\beta_m \bar{z}) \}. \tag{30}$$

The complex-valued Fourier series coefficients  $p_m$  and  $q_m$  in this extra term must be chosen so that to satisfy the conditions (27). To find them, we expand (29) into the Fourier series in  $x_1$ . By applying (A.2), we get for the singular part of  $T_n$ , namely  $T_s = T_n(u_s) = \sum_{p=1}^N T_n[u_{ps}(z_p)]$

$$\begin{aligned}
 T_s(z) &= \sum_{p=1}^N \sum_{m=0}^{\infty} \{ \exp(i\beta_m z) [(i\beta_m)^2 (\bar{z} - z - \bar{Z}_p + Z_p) P_m^{(p)+} + i\beta_m Q_m^{(p)+}] \exp(-i\beta_m Z_p) \\
 &\quad - \overline{i\beta_m \exp(i\beta_m z) P_m^{(p)+} \exp(-i\beta_m Z_p)} \}; \\
 T_s(z - bi) &= \sum_{p=1}^N \sum_{m=0}^{\infty} \exp(-\beta_m b) \{ \exp(-i\beta_m z) \\
 &\quad \times [(i\beta_m)^2 (\bar{z} - z + 2bi - \bar{Z}_p + Z_p) P_m^{(p)+} + i\beta_m Q_m^{(p)+}] \exp(i\beta_m Z_p) \\
 &\quad + \overline{i\beta_m \exp(-i\beta_m z) P_m^{(p)-} \exp(i\beta_m Z_p)} \};
 \end{aligned} \tag{31}$$

where

$$P_m^{(p)\pm} = \sum_{n=1}^{\infty} a_n^{(p)} t_{nm}^{\pm}, \quad Q_m^{(p)\pm} = \sum_{n=1}^{\infty} b_n^{(p)} t_{nm}^{\pm}. \tag{32}$$

After substitution (30) and (31) into (27), we obtain for  $m > 0$

$$\begin{aligned}
 p_{\pm m} &= \frac{1}{\Delta_m} \sum_{p=1}^N P_m^{(p)\pm} \exp(\mp i\beta_m Z_p); \\
 q_{\pm m} &= \frac{1}{\Delta_m} \sum_{p=1}^N \left\{ \left[ 2b \frac{\exp(\beta_m b)}{\Delta_m} \pm i(Z_p - \bar{Z}_p) \right] \beta_m P_m^{(p)\pm} + Q_m^{(p)\pm} \right\} \exp(\mp i\beta_m Z_p);
 \end{aligned} \tag{33}$$

where  $\Delta_m = \exp(2\beta_m b) - 1$ . Thus,  $p_m$  and  $q_m$  taken in the form (33) satisfy the boundary conditions (27) accurately. In turn, the edge disturbance  $u_h$  affects the stress field around inclusions and has to be taken into account as well by proper modification of the procedure described in the previous Section. By applying the formula (A.8) to (30) one finds easily the local expansion of  $u_h$  in a vicinity of  $Z_q$ :

$$u_h(z) = u_h(z_q + Z_q) = \varkappa_0 \varphi_{hq}(z_q) - (z_q - \bar{z}_q) \overline{\varphi'_{hq}(z_q)} - \overline{\psi_{hq}(z_q)}, \tag{34}$$

where

$$\varphi_{hq}(z_q) = \sum_{k=0}^{\infty} A_k^{(q)} (z_q)^k, \quad \psi_{hq}(z_q) = B_k^{(q)} (z_q)^k \tag{35}$$

and

$$\begin{aligned}
 A_k^{(q)} &= \sum_{m \neq 0} p_m \frac{(i\beta_m)^k}{k!} \exp(i\beta_m Z_q); \\
 B_k^{(q)} &= - \sum_{m \neq 0} [i\beta_m (Z_q - \bar{Z}_q) p_m - q_m] \frac{(i\beta_m)^k}{k!} \exp(i\beta_m Z_q).
 \end{aligned} \tag{36}$$

Remarkably, the local expansion (34) is identical in form to that of the regular part of (21). Hence, derivation of the resolving set of equations follows the same way as described above, with replace  $a_{-k}^{(q)}$  to  $(a_{-k}^{(q)} + A_k^{(q)})$  and  $b_{-k}^{(q)}$  to  $(b_{-k}^{(q)} + B_k^{(q)})$  and gives (24) with  $A_k^{(q)}$  and  $B_k^{(q)}$  standing in the right hand side

$$\begin{aligned}
 \frac{\Omega_1}{(R_q)^{2k}} [(R_q)^2 (k-2) a_{k-2}^{(q)} - (b_k^{(q)} + k a_k^{(q)})] + \overline{a_{-k}^{(q)}} &= -\delta_{k1} \Gamma_1 - \overline{A_k^{(q)}}; \\
 \frac{\Omega_2}{(R_q)^{2k}} a_k^{(q)} - (k+2) (R_q)^2 \overline{a_{k-2}^{(q)}} - (\overline{b_{-k}^{(q)}} - k a_{-k}^{(q)}) &= \delta_{k1} (\overline{\Gamma_2} - \Gamma_1) + (k+2) (R_q)^2 \overline{A_{k+2}^{(q)}} + \overline{B_k^{(q)}} - k A_k^{(q)};
 \end{aligned} \tag{37}$$

$$q = 1, 2, \dots, N; \quad k = 1, 2, \dots;$$

Eq. (37) together with (20), (22), (33) and (36) constitute a closed set of linear equations. Some additional analytical work, namely substitution of (32) into (33) and, then, into (36) and (37) allows to exclude the unknowns

$P_m^{(p)\pm}$ ,  $Q_m^{(p)\pm}$ ,  $p_m$ ,  $q_m$ ,  $A_k^{(q)}$  and  $B_k^{(q)}$  from the resolving set of equations and thus to reduce greatly the total computational effort.

### 3.3. Finite thickness composite ply

To be specific, we prescribe the kinematic boundary conditions on both flat edges of the ply (Fig. 4), namely

$$u_m|_{x_2=-b} = 0; \quad u_m|_{x_2=0} = i\delta. \tag{38}$$

and show how to provide them by proper taking the Fourier series coefficients  $p_m$  and  $q_m$  in the boundary-related term  $u_h$  (29). To find them, we note first that in our model  $-b < X_{2p} < 0$ ,  $p = 1, 2, \dots, N$ .

By definition,  $z = z_p + Z_p$ ; therefore,  $x_{2p} > 0$  for  $x_2 = 0$  (upper edge of layer) and  $x_{2p} < 0$  for  $x_2 = -b$  (bottom one). We expand (38) into a Fourier series in  $x_1$ . Applying (A.2), to the singular part of  $u_m$ , namely,  $u_s = \sum_{p=1}^N u_{ps}(z_p)$  gives us

$$\begin{aligned} u_s|_{x_2=0} &= \sum_{m=0}^{\infty} \left\{ \exp(i\beta_m x_1) \left[ \kappa_0 \sum_{p=1}^N P_m^{(p)+} \exp(-i\beta_m Z_p) \right] \right. \\ &\quad \left. + \exp(-i\beta_m x_1) \sum_{p=1}^N \left[ i\beta_m (\overline{Z_p} - Z_p) \overline{P_m^{(p)+}} - \overline{Q_m^{(p)+}} \right] \exp(i\beta_m \overline{Z_p}) \right\}; \\ u_s|_{x_2=-b} &= \sum_{m=0}^{\infty} \exp(-\beta_m b) \left\{ \exp(-i\beta_m x_1) \left[ \kappa_0 \sum_{p=1}^N P_m^{(p)-} \exp(i\beta_m Z_p) \right] \right. \\ &\quad \left. + \exp(i\beta_m x_1) \sum_{p=1}^N \left[ -\beta_m \langle 2b + i(\overline{Z_p} - Z_p) \rangle \overline{P_m^{(p)-}} - \overline{Q_m^{(p)-}} \right] \exp(-i\beta_m \overline{Z_p}) \right\}; \end{aligned} \tag{39}$$

where

$$P_m^{(p)\pm} = \sum_{n=1}^{\infty} a_n^{(p)} t_{nm}^{\pm}, \quad Q_m^{(p)\pm} = \sum_{n=1}^{\infty} b_n^{(p)} t_{nm}^{\pm}. \tag{40}$$

After substitution (30) and (39) into (38), we obtain for  $m > 0$

$$\begin{aligned} \kappa_0 p_m - \overline{q_{-m}} &= R_1; & \kappa_0 p_m \exp(2\beta_m b) - 2\beta_m b \overline{p_{-m}} - \overline{q_{-m}} &= R_3; \\ \kappa_0 p_{-m} - \overline{q_m} &= R_2; & \kappa_0 p_{-m} - (2\beta_m b \overline{p_m} - \overline{q_m}) \exp(2\beta_m b) &= R_4; \end{aligned} \tag{41}$$

where

$$\begin{aligned} R_1 &= -\kappa_0 \sum_{p=1}^N P_m^{(p)+} \exp(-i\beta_m Z_p); \\ R_2 &= \sum_{p=1}^N \left[ i\beta_m (\overline{Z_p} - Z_p) \overline{P_m^{(p)+}} - \overline{Q_m^{(p)+}} \right] \exp(i\beta_m \overline{Z_p}); \\ R_3 &= \sum_{p=1}^N \left[ -\beta_m \langle 2b + i(\overline{Z_p} - Z_p) \rangle \overline{P_m^{(p)-}} - \overline{Q_m^{(p)-}} \right] \exp(-i\beta_m \overline{Z_p}); \\ R_4 &= \kappa_0 \sum_{p=1}^N P_m^{(p)-} \exp(i\beta_m Z_p). \end{aligned} \tag{42}$$

By solving (41) for  $p_m$  and  $q_m$ , one finds

$$\begin{aligned} p_m &= \frac{\Delta_m \kappa_0 (R_3 - R_1) + 2\beta_m b \Delta_m \bar{R}_2 - 2\beta_m b (\bar{R}_4 - \bar{R}_2)}{(\Delta_m \kappa_0)^2 - [2\beta_m b \exp(2\beta_m b)]^2}; \\ q_m &= p_m 2\beta_m b \exp(2\beta_m b) / \Delta_m - (\bar{R}_4 - \bar{R}_2) / \Delta_m; \\ q_{-m} &= \kappa_0 \bar{p}_m - \bar{R}_1; \quad p_{-m} = (R_2 + \bar{q}_m) / \kappa_0; \end{aligned} \tag{43}$$

where  $\Delta_m = \exp(2\beta_m b) - 1$ .

The separate case is  $m = 0$ , where we have

$$\begin{aligned} u_m|_{x_2=0} - \frac{\pi i}{a} \sum_{p=1}^N (\kappa_0 a_1^{(p)} + b_1^{(p)}) &= i\delta; \\ u_m|_{x_2=-b} + \frac{\pi i}{a} \sum_{p=1}^N (\kappa_0 a_1^{(p)} + b_1^{(p)}) &= 0. \end{aligned} \tag{44}$$

From here, the constant term in  $u_m$  is

$$\Gamma_0 = i\delta + \frac{\pi i}{a} \sum_{p=1}^N (\kappa_0 a_1^{(p)} + b_1^{(p)}) \tag{45}$$

whereas the linear term coefficients  $\Gamma_1$  and  $\Gamma_2$  are given by

$$\Gamma_1 = \frac{E_{11} + E_{22}}{2(\kappa_0 - 1)}; \quad \Gamma_2 = \frac{1}{2}(E_{22} - E_{11} + 2iE_{12}), \tag{46}$$

with

$$E_{22} = \frac{\delta}{b} + \frac{2\pi}{ab} \sum_{p=1}^N (\kappa_0 a_1^{(p)} + b_1^{(p)}); \quad E_{ij} = 0 \quad (i, j \neq 2). \tag{47}$$

Thus,  $p_m$  and  $q_m$  chosen in the form (43) and  $\Gamma_i$  taken from (45)–(47) satisfy the boundary conditions (38) accurately. It is quite evident that the described procedure of executing the flat boundary conditions remains valid for any self-balanced set of loads, not violating the periodicity condition (4).

### 3.4. Effective stiffness

The stress field obtained from the above solution can be integrated analytically to get the closed form exact expression of the macroscopic, or effective, stiffness tensor  $C^*$  defined by

$$\langle \sigma_{ij} \rangle = C_{ijkl}^* \langle \varepsilon_{kl} \rangle, \tag{48}$$

where  $\langle \cdot \rangle$  means averaging over the RVE. In the model we consider, RVE coincides with the meso cell and, due to periodicity of structure,

$$\langle f \rangle = \frac{1}{V} \int_V f \, dV \tag{49}$$

where  $V$  is a cell volume. In our case,  $V = ab$  (unit length is assumed in  $x_3$ -direction).

In the problem we consider, the stress field is macroscopically homogeneous and governed either by the constant macroscopic strain  $\mathbf{E} = \{\langle \varepsilon_{ij} \rangle\}$  or stress  $\mathbf{S} = \{\langle \sigma_{ij} \rangle\}$  tensor. To evaluate  $\langle \varepsilon_{ij} \rangle$ , we write

$$\langle \varepsilon_{ij} \rangle = \frac{1}{2V} \int_V (u_{i,j} + u_{j,i}) \, dV = \frac{1}{2V} \left[ \left( \int_{V_m} + \sum_{p=1}^N \int_{V_p} \right) (u_{i,j} + u_{j,i}) \, dV \right], \tag{50}$$

where  $V_m$  is the matrix volume inside the cell and  $V_p = \pi R_p^2$  is the volume of  $p$ th fiber:  $V = V_m + \sum_{p=1}^N V_p$ . Now, we apply the Gauss' theorem to reduce the volume integrals to surface ones: taking into account also the first of adhesion conditions (2) we get

$$\langle \varepsilon_{ij} \rangle = \frac{1}{2V} \int_{\Sigma} (u_i n_j + u_j n_i) dS, \tag{51}$$

where  $\Sigma$  is the cell outer surface and  $n_i$  are the components of unit normal vector.

Evaluation of (2) uses periodicity property of  $u$ : so,

$$E_{11} = \frac{1}{V} \int_{\Sigma} u_1 n_1 dS = \frac{1}{V} \int_0^b [u_1(z+a) - u_1(z)] dx_2. \tag{52}$$

It follows from (29) and (14) that  $u_m(z+a) - u_m(z) = a(\kappa_0 \Gamma_1 - \Gamma_2)$ . Considering  $u_1 = \text{Re } u$  gives us

$$E_{11} = \text{Re}(\kappa_0 \Gamma_1 - \Gamma_2). \tag{53}$$

Similarly,

$$E_{22} = \frac{1}{V} \int_{\Sigma} u_2 n_2 dS = \frac{1}{V} \int_0^a [u_2(z+bi) - u_2(z)] dx_1, \quad u_2 = \text{Im } u_m; \tag{54}$$

based on the expansion (A.2), one finds

$$u_m(z+bi) - u_m(z) = bi(\kappa_0 \Gamma_1 - \overline{\Gamma_1}) - bi(\overline{\Gamma_1} - \overline{\Gamma_2}) - 2bi\Gamma_{\Sigma}, \tag{55}$$

and

$$E_{22} = \text{Re}[(\kappa_0 - 2)\Gamma_1 + \Gamma_2 - 2\Gamma_{\Sigma}], \quad \text{where } \Gamma_{\Sigma} = \frac{\pi}{V} \sum_{p=1}^N (\kappa_0 a_1^{(p)} + \overline{b_1^{(p)}}). \tag{56}$$

In the same way we obtain

$$E_{12} = \text{Im}(\Gamma_2 - \Gamma_1 + \Gamma_{\Sigma}). \tag{57}$$

From here we can derive the equations determining the parameters  $\Gamma_1$  and  $\Gamma_2$ :

$$\begin{aligned} (\kappa_0 - 1)\Gamma_1 &= \frac{E_{11} + E_{22}}{2} + \Gamma_{\Sigma}; \\ \Gamma_2 &= \Gamma_1 + \frac{E_{22} - E_{11}}{2} + iE_{12} + \overline{\Gamma_{\Sigma}}; \end{aligned} \tag{58}$$

and, thus, completing the problem statement.

Evaluating the macroscopic stress follows the same way:

$$\langle \sigma_{ij} \rangle = \frac{1}{V} \int_V \sigma_{ij} dV = \frac{1}{2V} \left[ \left( \int_{V_m} + \sum_{p=1}^N \int_{V_p} \right) 2G \left( \varepsilon_{ij} + \frac{\delta_{ij} \nu \theta}{1 - 2\nu} \right) dV \right]; \tag{59}$$

after some algebra, we come to

$$\begin{aligned} \frac{S_{ij}}{2G_0} &= E_{ij} + \delta_{ij}(E_{11} + E_{22}) + \sum_{p=1}^N \left[ (\tilde{G}_p - 1) \frac{f_p}{V_p} \int_{V_p} \varepsilon_{ij} dV \right. \\ &\quad \left. + \delta_{ij} \left( \tilde{G}_p \frac{\nu_p}{1 - 2\nu_p} - \frac{\nu_0}{1 - 2\nu_0} \right) \frac{f_p}{V_p} \int_{V_p} \theta dV \right], \quad f_p = \frac{V_p}{V} \end{aligned} \tag{60}$$

Thus, the problem is reduced to evaluating the

$$\frac{1}{V_p} \int_{V_p} \varepsilon_{ij} dV = \frac{1}{2\pi R_p^2} \int_{L_p} (u_i n_j + u_j n_i) dl = \frac{1}{2\pi R_p} \int_0^{2\pi} (u_i n_j + u_j n_i) d\varphi. \tag{61}$$

On the circle  $r_p = R_p$ ,  $n = n_1 + in_2 = \exp(i\varphi)$ ; with account for the explicit form (15), (16) of displacement inside the  $p$ th fiber, integration in (61) is rather trivial task leading to

$$\begin{aligned} \frac{1}{V_p} \int_{V_p} (\varepsilon_{11} + \varepsilon_{22}) dV &= 2(\varkappa_p - 1) \text{Rec}_{-1}^{(p)}; \\ \frac{1}{2V_p} \int_{V_p} (\varepsilon_{22} - \varepsilon_{11} + 2i\varepsilon_{12}) dV &= d_{-1}^{(p)} - c_{-1}^{(p)} + 3R_p^2 c_{-3}^{(p)}. \end{aligned} \tag{62}$$

Combining (62) and (60) gives us an explicit expression of (48) written in compact form as

$$\begin{aligned} \frac{S_{11} + S_{22}}{2G_0} &= \frac{E_{11} + E_{22}}{(\varkappa_0 - 1)} + \sum_{p=1}^N 2f_p \left( \tilde{G}_p \frac{v_p}{1 - 2v_p} - \frac{v_0}{1 - 2v_0} \right) (\varkappa_p - 1) \text{Rec}_{-1}^{(p)}; \\ \frac{S_{22} - S_{11} + 2iS_{12}}{2G_0} &= E_{22} - E_{11} + 2iE_{12} + \sum_{p=1}^N 2f_p (\tilde{G}_p - 1) (d_{-1}^{(p)} - c_{-1}^{(p)} + 3R_p^2 c_{-3}^{(p)}). \end{aligned} \tag{63}$$

As a last step, we utilize the relations (26) to express  $S_{ij}$  in terms of variables  $a_n^{(p)}$  and  $b_n^{(p)}$  entering the resolving system (24) and get the final exact, finite-form result:

$$\begin{aligned} \frac{S_{11} + S_{22}}{2G_0} &= \frac{E_{11} + E_{22}}{(\varkappa_0 - 1)} + \frac{2\pi}{V} \frac{(\varkappa_0 + 1)}{(\varkappa_0 - 1)} \sum_{p=1}^N (a_1^{(p)} + b_1^{(p)}); \\ \frac{S_{22} - S_{11} + 2iS_{12}}{2G_0} &= E_{22} - E_{11} + 2iE_{12} + \frac{2\pi}{V} (\varkappa_0 + 1) \sum_{p=1}^N a_1^{(p)}. \end{aligned} \tag{64}$$

Together with (48), these relations enable evaluation of all the transverse effective stiffness moduli.

## 4. Numerical study

### 4.1. Numerical realization and efficiency

The series solution we derive above is an accurate, asymptotically exact one. This means that, in order to get the exact values, one has to solve a whole infinite set of linear equations. In practice, it is solved by applying the truncation method which means that only a certain *finite* number  $N_{\text{eqn}}$  of equations and unknowns is retained in (37). Based on asymptotic analysis of the linear set (37), it can be proven rigorously (Kantorovich and Krylov, 1964) that an approximate solution obtained in this way converges to an exact one with  $N_{\text{eqn}} \rightarrow \infty$ . Thus, any desirable accuracy can be achieved by the proper choice of  $N_{\text{eqn}}$ .

Noteworthy, numerical realization of the developed method is rather simple. The matrix coefficients of the linear system are given by the simple rational expressions and, unlike FEM or BEM, involve no integration. Instead, they contain the ordinary rapidly convergent infinite sums, which can be expressed in terms of Euler zeta-function  $\zeta(n)$  tabulated elsewhere (e.g., Abramovitz and Stegun, 1964). In fact, the most computational time is spent by the linear solver and, to provide the best performance, the proper solver must be chosen. The well known fact is that the CPU time for the direct and iterative solvers scales as  $O(N_{\text{eqn}}^3)$  and  $O(N_{\text{eqn}}^2)$ , respectively. Moreover, for the typical in the many-fiber models large ( $N_{\text{eqn}} > 1000$ ) sets of equations the direct solvers are not welcome due to substantial numerical error accumulation; the iterative solvers are preferable if not the only choice. Among them, the generalized minimum residuals (GMRES) algorithm by Saad and Schultz (1986) was reported by many authors as the best compatible with the multipole expansion technique. A convergence rate (and hence numerical efficiency) of GMRES depends on the rational choice of preconditioner matrix and initial guess. Preconditioning involves multiplication of both sides of (37) by a matrix  $\mathbf{P}$ , the preconditioner. Following Fu et al. (1998), we choose  $\mathbf{P}$  to be block-diagonal, with each block being equal to the inverse of the corresponding diagonal block of the matrix (37). Formally, this preconditioner is known as block-Jacobi. For many-particle problems, the block-Jacobi preconditioner has a clear physical meaning: it exactly represents the solution for non-interacting fibers.

In this work, the open source Fortran code of GMRES routine by Fraysse et al. (1998), with minor modifications, is utilized. Some idea of its numerical efficiency can be drawn from Table 1, where the run time vs number of equations  $N_{\text{eqn}}$  is given for three double precision linear solvers. They are: DLAX, standard direct

Table 1  
Linear solver elapsed time, s

$N_{\text{eqn}}$	DLAX	DLSARG	GMRES
1600	9.5	3.0	0.43
2400	31.9	8.6	0.94
3600	79.1	40.5	1.8
4800	Lost accuracy	100.1	4.2

solver (SSL2 library, Lahey Fortran 5.7); DLSARG, standard direct solver (IMSL library, Compaq Visual Fortran 6.5) and GMRES, the problem-adjusted iterative solver. All the subsequent numerical data have been obtained using the Pentium IV 2.4 GHz single processor PC. It is seen quite clearly from the table that using the standard direct solvers has no perspective. Yet another argument in favor of using the iterative solver for the progressive damage simulation consists in that the solution obtained on the previous step represents a natural initial guess for the next step: doing so results in the rapid convergence of iterations. The further improvement of numerical performance can be achieved by taking the more elaborated preconditioner  $\mathbf{P}$  and by allowing the algorithm to automatically adjust the number of terms in Fourier series in order to reach the desirable level of accuracy.

Also, it is of interest to make comparison with the similar works where the numerical effort is reported. Say, [Chen and Papathanasiou \(2004\)](#) have used the parallel BEM implementation showing, as they claim, better performance in comparison with FEM. They reported that a typical run for the model with 144 fibers and minimum inter-fiber distance  $\delta_{\min} = 0.05$ , discretized with  $\sim 4000$  quadratic elements, took approximately 15 min on the eight-processor grid, 120 min in total. Unfortunately, they did not report the used processor type/performance rate and dimension of the set of equations they solved. The time spent by our code to solve the model BVP with the same parameters (144 fibers,  $\delta_{\min} = 0.05$ ) and  $N_{\text{eqn}} = 14,400$  ranges from 1 to 2 min depending on the fiber volume content which means that the developed method is almost two orders more efficient in comparison with the mentioned above numerical code.

An efficient, fast multipole-based algorithm for studying the large-scale models has been developed recently by [Wang et al. \(2005b\)](#). The plotted there in [Fig. 8](#) CPU time vs number of degree of freedom gives the estimated run time of 100 s for  $N_{\text{eqn}} = 14,400$  which is remarkably close to that obtained by us. It is not surprising, however, because the underlying mathematical theory of compared works is rather similar. And, even more pronounced speedup effect can be achieved by combining these two techniques, namely, the fast multipole expansion and periodic singular potentials, see, e.g., [Sangani and Mo \(1996\)](#) and [Kushch et al. \(2002\)](#).

#### 4.2. Convergence

Three main parameters governing convergence and accuracy of results in the below statistical analysis are

- number  $N_{\text{harm}}$  of harmonics retained in the series expansions (13) and (16);
- number  $N_{\text{fib}} = N$  of fibers with the centers lying inside the unit cell;
- number  $N_{\text{conf}}$  of random structure realizations taken for averaging.

Obviously, all these numbers should be taken sufficiently large to provide the reliable numerical results. On the other hand, computational effort of such a study scales as  $(N_{\text{eqn}})^{\alpha} N_{\text{conf}}$ , where number of equations  $N_{\text{eqn}} = 4N_{\text{fib}}N_{\text{harm}}$  and  $\alpha = 2$  or  $3$  depending on the linear solver type (iterative or direct, respectively) utilized and, to avoid exceedingly large total computational time, the reasonable values of  $N_{\text{harm}}$ ,  $N_{\text{fib}}$  and  $N_{\text{conf}}$  are to be taken. Their motivated choice can be made based on the solution convergence rate study.

First, we evaluate number of harmonics  $N_{\text{harm}}$  we need to keep in the numerical solution in order to get the convergent solution. Specifically, we consider uniaxial tension  $S_{22} = 1$  of a composite with the equal-sized fibers of diameter  $D$ . The elastic properties of composite phases are  $E_0 = 3.2$  GPa,  $\nu_0 = 0.36$ ,  $E_p = 3.2$  GPa,  $\nu_p = 0.25$  ([Meraghni et al., 2002](#)); hence,  $G_p = 24G_0$ ,  $p = 1, 2, \dots, N$ . Some idea of convergence rate can be

Table 2  
 $\sigma_{r \max}$  at interface: two inclusions along the loading direction

$N_{\text{harm}}$	$\delta_{\min}$			
	0.5	0.2	0.05	0.02
10	2.00	2.75	4.32	26.3
20	2.00	2.76	4.25	5.55
30	2.00	2.76	4.25	5.19
40	2.00	2.76	4.25	5.18

Table 3  
 $\sigma_{r \max}$  at interface: a square array of inclusions

$N_{\text{harm}}$	$\delta_{\min}$			
	0.5 ( $c = 0.349$ )	0.2 ( $c = 0.545$ )	0.05 ( $c = 0.712$ )	0.02 ( $c = 0.755$ )
10	1.53	1.74	2.88	2.26
20	1.53	1.72	2.29	2.66
30	1.53	1.72	2.28	2.69
40	1.53	1.72	2.28	2.70

drawn from Tables 2 and 3, where the interface stress  $\sigma_{r \max} = \max_{0 < \varphi < 2\pi} \sigma_r$  is given as a function of  $\delta_{\min}$  and  $N_{\text{harm}}$ .

Not surprisingly, stress concentration caused by two fibers in otherwise homogeneous matrix is higher because in the composite, for the equal far load, the smaller strain and, hence, lower local stress develops. The data shown in Table 4 were obtained for the random structure realization (30 inclusions per cell) with  $\delta_{\min} = 0.02$ ; the fiber volume content  $c = \sum_{p=1}^N V_p / V$  was taken the same as in Table 3. Here, no smooth  $\sigma_{r \max}(c)$  dependence is expected because, for each  $c$ , only one random structure realization was taken. However, the max stress decreasing tendency is quite clear: the higher is the fiber volume content, the less room left for isolated clusters of a few fibers where the highest interface stress concentration is most probable.

In Fig. 5, the  $\sigma_r$  stress variation along the interface of the arbitrarily chosen fiber in the model with 30 fibers per cell,  $c = 0.349$  and already  $N_{\text{harm}} = 20$  gives the practically convergent solution with a relative error in stress below 1%. Obviously, the smaller is  $\delta_{\min}$ , the stiffer is the model BVP (no matter, analytical or numerical method we apply to solve it) and the higher local stress concentration is expected. By prescribing a fixed allowable distance  $\delta_{\min}$ , we, in fact, pre-determine the maximum allowable stress and to be consistent with practice, this parameter should be taken as small as possible. Some idea of how  $\sigma_{r \max}$  can be affected by  $\delta_{\min}$  can be drawn from the stress asymptotics for nearly touching fibers.

It worth to mention here that the developed analytical method is also advantageous in that it (BEM and FEM unlike) handles equally well the problems with separated and touching inclusions.

It is seen from Fig. 6 that the interface stress remains finite when the fibers are drawn together ( $\delta_{\min} \rightarrow 0$ ). This is the well-known problem: the stress singularity is expected only in the case of rigid (non-deformable) inclusions.

The lines represent our solution where, in the case of a finite array of inclusions, the periodic part is omitted:  $H_{nm}^* = H_{nm}$ . The analogous data obtained by FEM are shown in the plot by the solid circles for two fibers and by the open circles for a square array of fibers. As seen from the plot, the compared data practically

Table 4  
 $\sigma_{r \max}$  at interface of the arbitrarily chosen fiber: quasi-random array of inclusions

$N_{\text{harm}}$	$c$			
	0.349	0.545	0.712	0.755
10	8.00	5.36	5.38	6.47
20	3.90	3.50	2.59	2.73
30	3.88	3.50	2.57	2.72
40	3.88	3.50	2.57	2.72

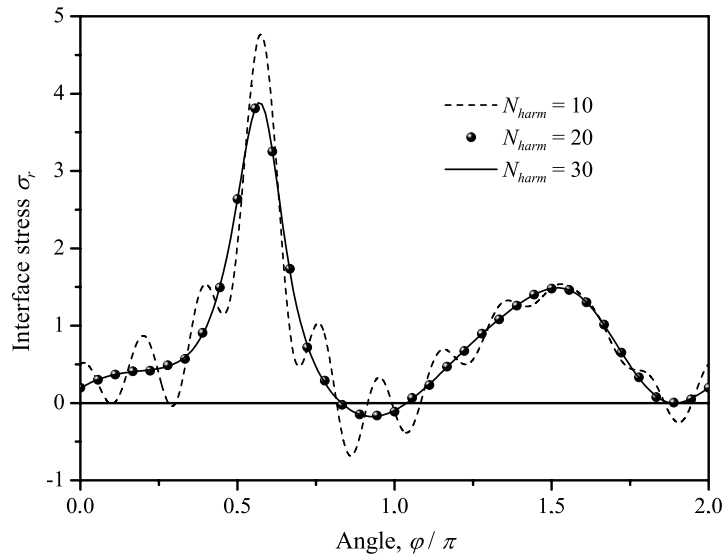


Fig. 5. Interface stress convergence with  $N_{\text{harm}}$  increased.

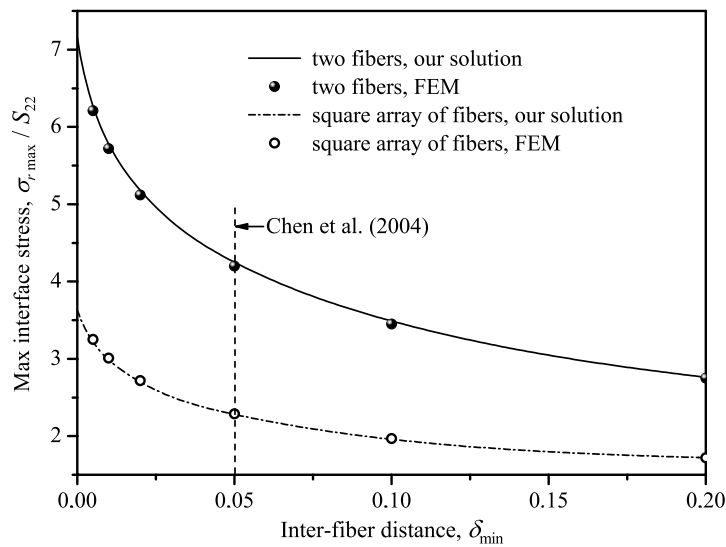


Fig. 6. Max interface stress as a function of normalized inter-fiber distance.

coincide which validates both the developed theory and numerical code. Noteworthy, for  $\delta_{\text{min}} = 0.05$  adopted by [Chen and Papathanasiou \(2004\)](#) the probable  $\sigma_{r,\text{max}}$  underestimation is almost two times. In the subsequent numerical study, we put  $\delta_{\text{min}} = 0.01$  which seems to be a reasonable compromise between the accuracy and computational effort.

The next issue is a number of fibers  $N_{\text{fiber}}$  inside the unit cell. The data in [Table 5](#) are the mean stress inside the cell, averaged over 50 configurations and given in the form  $\langle \sigma_{ij} \rangle / C_{ijkl}^0 = M \pm S$ , where  $M$  and  $S$  are the

Table 5  
Effective stiffness of a fibrous composite: convergence and isotropy checking

	$\langle \sigma_{11} \rangle / C_{1111}^0$	$\langle \sigma_{22} \rangle / C_{2222}^0$	$\langle \sigma_{12} \rangle / C_{1212}^0$
$N = 20, E_{11} = 1$	$2.685 \pm 0.016$	$2.242 \pm 0.012$	$0.009 \pm 0.012$
$N = 20, E_{22} = 1$	$2.242 \pm 0.011$	$2.659 \pm 0.016$	$0.009 \pm 0.012$
$N = 50, E_{11} = 1$	$2.683 \pm 0.011$	$2.270 \pm 0.008$	$-0.006 \pm 0.008$
$N = 50, E_{22} = 1$	$2.271 \pm 0.008$	$2.671 \pm 0.010$	$-0.005 \pm 0.009$

mean value and the standard error of the mean, respectively. Taking account of that loading is the uniaxial macroscopic strain  $E_{kl} = 1$ , these numbers are the nothing else than the effective elastic moduli of a fibrous composite:  $C_{ijkl}^* = \langle \sigma_{ij} \rangle |_{E_{kl}=1}$ . It is seen from the table that the values obtained for  $N_{\text{fib}} = 20$  and  $N_{\text{fib}} = 50$  are rather close which clearly indicates convergence of solution with respect to  $N_{\text{fib}}$ . These data can also be useful in verifying isotropy of the random structure model. Ideally, one must get for macroscopically isotropic composite material  $\langle \sigma_{11} \rangle |_{E_{11}=1} = \langle \sigma_{22} \rangle |_{E_{22}=1}$ ,  $\langle \sigma_{22} \rangle |_{E_{11}=1} = \langle \sigma_{11} \rangle |_{E_{22}=1}$  and  $\langle \sigma_{12} \rangle \equiv 0$ . As calculations show, already for  $N_{\text{fib}} = 20$  an anisotropy degree is below 1% and shows a clear tendency to decrease with the  $N_{\text{fib}}$  growing up.

The next figure shows how much a number of realizations  $N_{\text{conf}}$  affects the results of statistical averaging. In Fig. 7, the normalized effective Young modulus  $E_{\text{eff}}/E_0$  averaged over a number of random structure realizations is shown. The open circles correspond to  $N_{\text{fib}} = 20$  whereas the solid circles correspond to  $N_{\text{fib}} = 50$ . Based on these observations, the conclusion can be drawn that  $N_{\text{conf}} = 50$  provides practically convergent solution.

Of course, these data must be considered only as the indicative ones because they depend on the volume content of fibers, fiber-to-matrix moduli ratio, microstructure type, etc. In each specific case, the similar study must be done and the appropriate  $N_{\text{harm}}$ ,  $N_{\text{fib}}$  and  $N_{\text{conf}}$  numbers ensuring the accurate and statistically meaningful results should be determined.

### 4.3. Interface stress statistics

Now, we show a few results on the interface stress distribution obtained by the numerical experiments with  $N_{\text{fib}} = 100$  and  $N_{\text{harm}} = 20$ . In Fig. 8, a meso cell with the fiber volume content  $c = 0.5$  is shown. The shades of gray indicate peak interface stress level: the fibers with low peak stress are shown by dark, the heavily loaded fibers are shown by light gray color. It is clearly seen from the picture that  $\sigma_{r, \text{max}}$  varies greatly from one fiber to another. Visual observation easily discovers presence of the fiber chains with high  $\sigma_{r, \text{max}}$  oriented predominantly in the loading ( $x_2$ , in our case) direction. Reported earlier by Babuška et al. (1999), this clustering-related phenomenon is quite expectable in view of the above stress analysis. As numerical study shows, there always exists relatively small volume fraction of fibers with rather high interface stress concentration. Expectedly (see Fig. 6), the max stress is generated between the closely placed and oriented along the loading direction fiber pairs and this local stress greatly exceeds the mean value.

As to the  $\sigma_{r, \text{max}}$  statistical distribution rule, some idea of it can be drawn from Fig. 9, where the data for a composite with  $c = 0.5$  are shown. Here, the open circles represent empirical cumulative distribution for a single random structure realization, the solid circles are obtained by averaging over 10 runs. The solid line is the

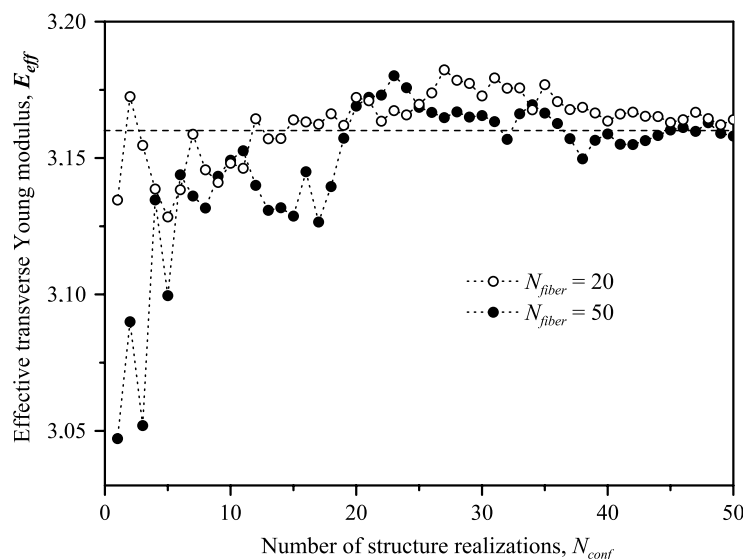


Fig. 7. Convergence of effective transverse Young modulus  $E_{\text{eff}}$  of FRC ( $c = 0.5$ ) with a number of realizations  $N_{\text{conf}}$  increased.

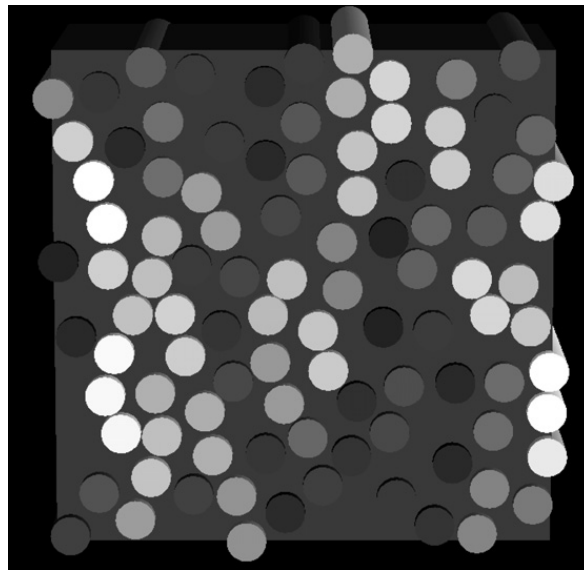


Fig. 8. Formation of the fiber chains with high interface stress (dark fibers, low stress; light fibers, high stress).

approximation of stress distribution by the “chain of bundles” model (see Gumbel, 1958; Ruggieri et al., 1995)  $y = \exp(-\exp(-k(x - x_c)))$ , where  $x_c = 1.53$  and  $k = 1.59$ . Claimed by Chen and Papathanasiou (2004) the Weibull’s statistics of max stress (dash-dotted line in Fig. 9) works only when the fibers are well separated ( $\delta_{\min} \geq 0.05$ ) and the interface stress are relatively low. In our case  $\delta_{\min} = 0.01$ , it approximates satisfactory only the low end of the empirical cumulative curve and not able to account for the peak stress predetermining initiation and accumulation of damage. Noteworthy, the  $\langle \sigma_{r \max} \rangle$  for the random structure composite is substantially higher than for the ordered square and, especially, hexagonal structure which can be regarded as “perfect” for the unidirectional FRC.

Obtained by averaging over all the fibers in each of 10 configurations the mean stresses  $\langle \sigma_{r \max} \rangle$  and  $\langle \varphi_{\max} \rangle$  as well as their standard deviations for a set of  $c$  value are given in Table 6. Here,  $\varphi_{\max}$  is the angle coordinate of the point at the matrix–fiber interface where the peak stress is attained. With  $c$  increased, the mean value  $\langle \sigma_{r \max} \rangle$  as well as its scattering is growing up; at the same time, the peak  $\sigma_{r \max}$  value is decreasing. Expectedly,

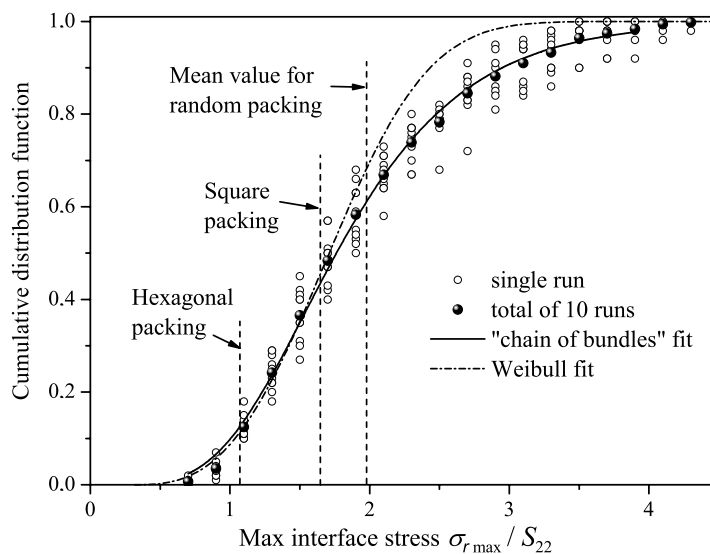


Fig. 9. Cumulative probability function of max  $\sigma_r$  distribution ( $c = 0.5$ ).

Table 6  
Mean value and standard deviation (SD) for  $\sigma_{r \max}$  and angle  $\varphi_{\max}$

$c$	$\langle \max \sigma_r \rangle$	SD	$\langle \varphi \rangle$	SD	$y = \exp\{-\exp[-k(x^a - x_c)]\}$		
					$k$	$x_c$	$a$
0.1	1.56	0.40	1.57	0.17	324	1.006	0.0222
0.2	1.67	0.60	1.55	0.21	310	1.004	0.0137
0.3	1.79	0.68	1.58	0.25	41.2	1.026	0.0789
0.4	1.90	0.75	1.58	0.28	3.91	1.231	0.552
0.5	1.98	0.74	1.54	0.30	1.68	1.554	0.975
0.5	2.01	0.66	1.57	0.34	1.14	1.922	1.276

the mean angle value  $\langle \varphi_{\max} \rangle = \pi/2$ ; its standard deviation is also growing up together with the fiber packing density.

Cumulative probability function of max  $\sigma_r$  distribution for a series of  $c$  value is given in Fig. 10. It is clearly seen from the plot that, regardless of  $c$ , there exists a relatively small fraction of fibers with rather high, comparable with that for two touching fibers, interface stress. In terms of the fatigue strength this means that debonding will occur in these “hot spots” much earlier than in all other sites. This correlates well with – and can be quite plausible explanation of – the experimentally observed (Brøndsted et al., 1997; Talreja, 2000, among others) rapid FRC stiffness degradation at the initial stage of cyclic loading. Needless to say, this effect can be properly modeled only if we take realistic, i.e., sufficiently small  $\delta_{\min}$ . The fitting function is the modified “chain of bundles”  $y = \exp\{-\exp[-k(x^a - x_c)]\}$  model; the coefficients  $k, a$  and  $x_c$  are given in Table 6. For the angle statistics, Lorenz’ distribution with the probability density  $y = 2Aw/\{\pi[4(x - x_c)^2 + w^2]\}$  and  $x_c = \pi/2$  seems to be appropriate approximation, see Fig. 11.

The presented above numerical examples are aimed primarily to demonstrate potential of the developed approach in the statistical study of FRC micro stress fields. An importance of these and other relevant relationships which can be obtained in this way consists in the following. The ultimate goal of our simulations is to develop the micro mechanics-based composite strength theory. To accomplish it, we need to link the micro structure parameters to the micro stress statistics and micro damage initiation and accumulation rate. The statistical parameters of an actual FRC micro structure and the constants entering the micro stress distribution functions we found from the numerical experiments could serve as the input variables of such a theory.

4.4. Application: simple debonding path model

Now, we give some idea of how numerical efficiency of our method can be utilized for simulating progressive damage in FRC. First, we assign the matrix–fiber interface to be the “weakest link”. The constant

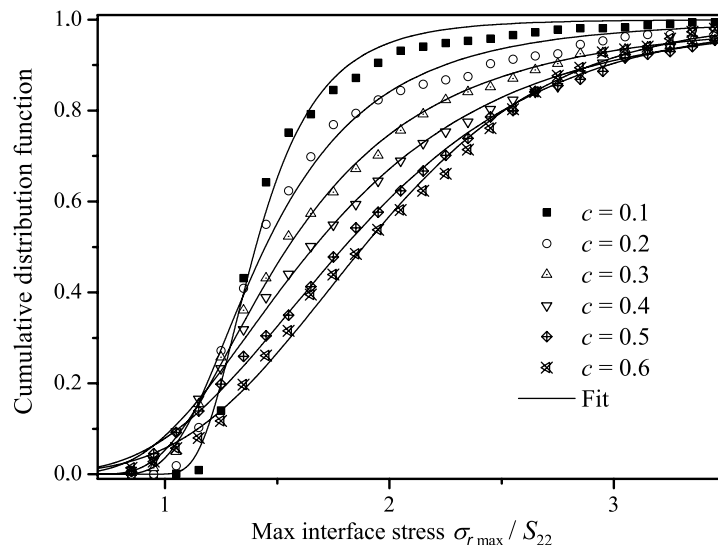


Fig. 10. Cumulative probability function of max  $\sigma_r$  distribution ( $c = 0.5$ ).

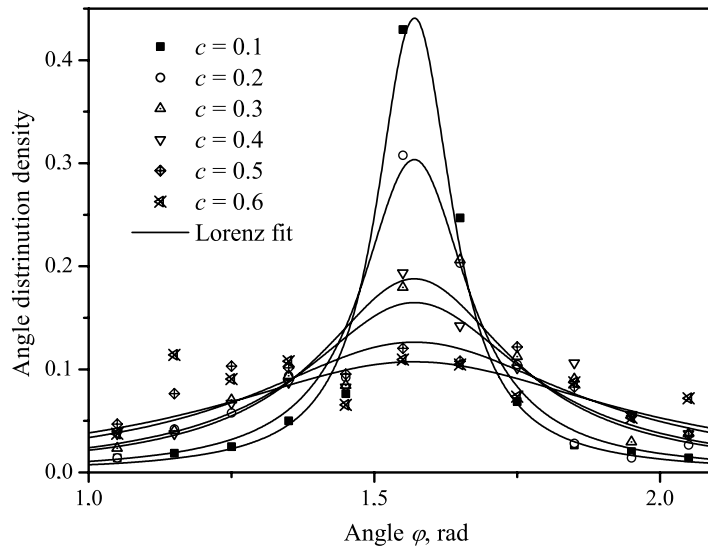


Fig. 11. Angle statistics (approximation – Lorenz' distribution).

amplitude cyclic load applied to the composite part results in the continuous sub micro damage accumulation and dropping down the interface strength  $S = S(N)$ . The debonding occurs when the condition  $\sigma_{r \max} = S(N)$  is satisfied at the most heavily loaded fiber. An instantaneous and complete fiber debonding is assumed: in our model, the debonded fiber is replaced with a pore and the modified model BVP is solved again, etc. Of course, this is obvious over-simplification: in a real composite, the partially and even fully debonded fiber may still contact the matrix and thus affect the local stress field and overall elastic response. There is a number of publications (Meraghni et al., 1996; Zheng et al., 2003; Gorbatkikh et al., 2005, among others) where these effects were studied; taking account of them represents a natural next step in development of our meso cell model but lies out of scope of this paper.

However, even in the framework of this simplest debonding model, some qualitative results can be obtained. In Fig. 12, the typical debonding fiber paths in the FRCs of regular (square and hexagonal) structure obtained by the described above step-by-step “progressive damage modeling” algorithm. In the perfectly bonded composite of regular structure, the stress field is the same in and around each fiber, therefore we artificially introduce the local defect (a single debonded fiber). It causes the local stress redistribution between the adjacent fibers, so the next and all subsequent debonding fibers are determined uniquely based on the above mentioned criterion. It is seen that the debonded fibers form a chain oriented transversely to the loading direction: for a square array (Fig. 12(a)), this chain is a straight line row whereas in the hexagonal structure a zig-zag-like chain, with more fibers involved is formed.

Not surprisingly, the same debonding pattern is observed in the random structure FRC. In Fig. 13(a) the typical simulation result is shown whereas Fig. 13(b) shows the experimentally observed (Gamstedt and

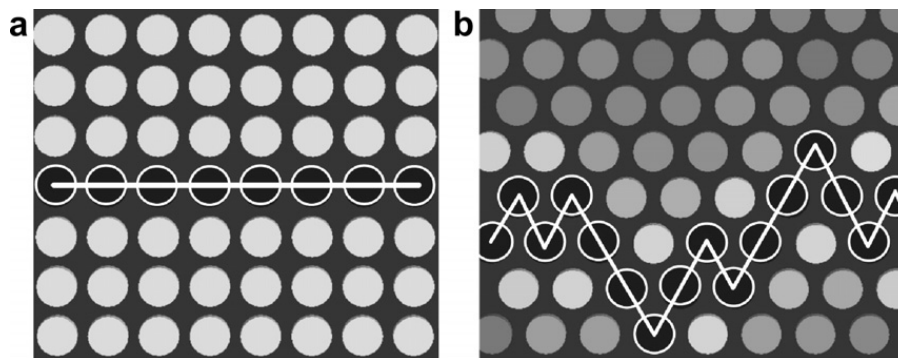


Fig. 12. Debonding path in the regular structure FRC: (a) – square, (b) – hexagonal packing.

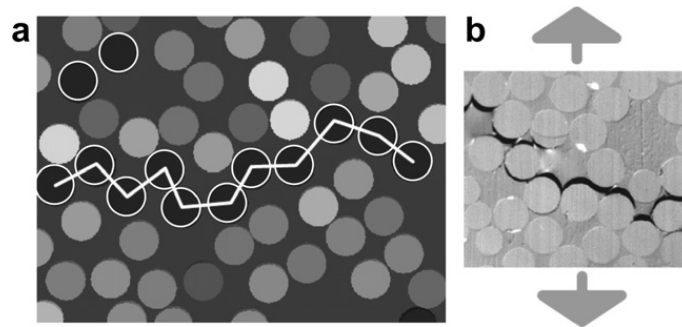


Fig. 13. Debonding path in the random structure FRC: (a) – simulation, (b) – experiment by Gamstedt and Andersen (2001). (b) is reproduced with kind permission from the authors.

Andersen, 2001) crack path; the similar data were obtained by many authors (see, e.g., Tsai, 1988). As seen from the plot, our simple model predicts correctly direction of damage development. In order to get a quantitative estimate of damage in terms of applied loads, number of cycles, stiffness reduction, etc., an additional effort in development of the model must be made including an account for imperfect interfaces, matrix cracking, delamination and other fatigue damage events. In fact, the chains of debonded fibers in the intact matrix are possible only where the interface is much weaker than matrix. According to the reported in the literature data, a majority of real-life composites possess a comparable matrix and interface strength (at least, of the same order of magnitude). Therefore, most likely, one of two “destructive” scenarios will be realized.

Let us consider, for the sake of simplicity, the defect-free composite with the fibers arranged in the square array,  $c = 0.5$ , subject to uniaxial tension  $S_{22} = 1$ . Induced by it the interface stress concentrations are  $\sigma_{r \max} = 1.64$  and  $\sigma_{\varphi \max} = 0.89$ . After complete debonding the test fiber and replacing it with a pore, we get  $\sigma_{r \max} = 0$  and  $\sigma_{\varphi \max} = 1.58$ ; it means that with a comparable probability one can expect the matrix failure nearby the appeared pore. After debonding in the same way one more, neighbor in  $x_1$ , fiber we obtain  $\sigma_{\varphi \max} = 2.34$  and this stress is localized in the bridge separating two pores. It is natural to expect the inter-pore crack formation and propagation in the direction, transversal to the loading axis.

More probable is the second scenario, because our “complete debonding” assumption is hardly realistic. A newly originated interface crack is approximately perpendicular to the loading direction (more precisely, to the traction acting at interface). With the crack propagating along the interface, an angle between the crack tip and the loading axis is decreased: intuitively evident that the crack “motivation” to propagate along interface is dropping down as well. At the same time, the hook stress is growing up, hence, one can expect kinking the crack into the matrix, toward another pore/crack (Prasad and Simha, 2003; Paris et al., 2007) and the macro crack formation (Fig. 13b). To be able simulate these and other relevant fatigue damage phenomena and to obtain a quantitative estimate of stiffness degradation due to interface debonding, our model must be generalized on the case of imperfect interfaces. One promising way to account for the interface defects has been suggested by Gorbatkikh et al. (2005) and another – by Crouch and Mogilevskaya (2006). Both they can be readily incorporated in the developed by us solving technique; however, this is a topic of a separate paper.

## 5. Conclusions

An accurate analytical method has been developed to solve for stress in an infinite quasi-random array of circular inclusions embedded in the matrix, the last being a “meso cell” model of disordered fibrous composite. Up to several hundred of interacting fibers can be considered in the model which is sufficient to account for the micro structure statistics of a real composite. The method combines technique of periodic complex potentials with the Fourier series expansion and re-expansion formulae and can be thought as a version of the multipole expansion method. The developed theory allows to reduce the primary boundary-value problem of the elasticity theory for a multiple-connected domain to an ordinary well-posed set of linear algebraic equations. Together with the properly chosen iterative solver,

it provides rather high numerical efficiency of the method, which makes it potentially efficient tool for studying progressive damage in FRCs. The results of numerical study are given on the interface stress statistics and fiber debonding paths development and they appear to correlate well with the experimental observations.

### Acknowledgement

The support by the Commission of the European Communities through the Sixth Framework Programme Grant UpWind.TTC (Contract #019945) is greatly acknowledged.

### Appendix A. Periodic potentials

Let us consider the functions defined by the convergent series

$$t_n(z) = \sum_{k=-\infty}^{\infty} \frac{1}{(z - ka)^n}, \quad n = 1, 2, \dots \quad (\text{A.1})$$

These functions are periodic in  $x_1$  with period  $a$  and possess a countable set of  $n$ th order poles in the points  $z = ka$ . For  $x_2 \neq 0$  these functions are continuous and, thus, allow expansion into the Fourier series with respect to  $x_1$ . It has been found elsewhere (Golovchan et al., 1993) that these series expansions have the form

$$t_n(z) = \sum_{m=0}^{\infty} t_{nm}^{\pm} \exp(\pm i\beta_m z), \quad x_2 \gtrless 0; \quad (\text{A.2})$$

where  $\beta_m = 2\pi m/a$  and  $t_{nm}^{\pm} = \frac{2\pi}{a} \varepsilon_m (\beta_m)^{n-1} \frac{(\mp i)^n}{(n-1)!}$ ;  $\varepsilon_0 = \frac{1}{2}$ ,  $\varepsilon_m = 1$  for  $m > 1$ .

The expressions (A.2) are particularly useful when it comes to executing the boundary conditions at the flat boundaries  $x_2 = \text{const}$ . It is clear from (A.2) that  $t_n(z) \rightarrow 0$  when  $|x_2| \rightarrow \infty$  for all  $n > 1$ , whereas  $t_1(z) \rightarrow t_{10}^{\pm} = \mp 2\pi i/a$  as  $x_2 \rightarrow \pm\infty$ . Thus, the functions (A.1) can be thought as singular periodic potentials whereas the functions  $\exp(\pm i\beta_m z)$  may be considered as the regular periodic potentials for a half plane.

On the other hand, to fulfil the matrix–fiber interface conditions (2), the functions (A.1) are to be expanded into Laurent power series around a certain point. These expansions can be obtained by applying term wise the formula

$$\frac{1}{(z + Z)^n} = \sum_{k=0}^{\infty} H_{nk}(Z) z^k, \quad H_{nk}(Z) = (-1)^k \frac{(n+k-1)!}{k!(n-1)!} Z^{-(n+k)}. \quad (\text{A.3})$$

followed by a proper change of summation order. So, local expansion around the pole  $z = 0$  is given by

$$t_n(z) = \frac{1}{z^n} + \sum_{m=0}^{\infty} H_{nm}^*(0) z^m, \quad |z| < a; \quad (\text{A.4})$$

where

$$H_{nm}^*(0) = \sum_{k \neq 0} H_{nm}(ak) = [(-1)^n + (-1)^m] \frac{(n+m-1)!}{m!(n-1)!} \zeta(n+m). \quad (\text{A.5})$$

With the fact that  $\zeta(n) = \sum_{k=1}^{\infty} \frac{1}{k^n}$  is the Euler  $\zeta$ -function taken into account, evaluation of (A.5) is rather simple: first,  $H_{nm}^*(0) \equiv 0$  for  $(n+m)$  odd. Then,  $\zeta(2) = \pi^2/6$  and  $\zeta(4) = \pi^4/90$  (Abramovitz and Stegun, 1964); for  $(n+m) \geq 6$  direct summation is rapid.

Local expansion of  $t_n(z_p)$  in a vicinity of the regularity point  $z_q$  can be written in the following, convenient for subsequent usage form:

$$t_n(z_p) = \sum_{m=0}^{\infty} H_{nm}^*(Z_{pq}) z_q^m, \quad z_p = z_q + Z_{pq} \quad (Z_{pq} \neq ka); \quad (\text{A.6})$$

where now

$$H_{nm}^*(Z_{pq}) = \sum_k H_{nm}(Z_{pq} - ak) = (-1)^m \frac{(n+m-1)!}{m!(n-1)!} t_{n+m}(Z_{pq}). \quad (\text{A.7})$$

To evaluate  $t_{n+m}(Z_{pq})$  numerically, three following case-dependent methods are applicable:

- (a) direct summation provided  $(n+m)$  is sufficiently large; otherwise;
- (b) Fourier series expansion (A.2), if  $|X_{2pq}| > \delta$ ; and, the last;
- (c) expansion of type (A.4) in the case  $|X_{2pq}| \leq \delta$ .

Local expansion of the “half plane” regular potentials  $\exp(\pm i\beta_m z)$  is rather simple:

$$\exp(\pm i\beta_m z) = \sum_{k=0}^{\infty} \frac{(\pm i\beta_m)^k}{k!} z^k. \quad (\text{A.8})$$

## References

- Abramovitz, M., Stegun, I.A., 1964. Handbook for mathematical functions. In: NBS Applied Mathematics Series, vol. 55. Flammarion, Paris.
- Allen, D.H., Highsmith, A.L., Lo, D.C., 1990. A continuum damage mechanics model for life prediction of laminated composites. In: Cardon, A.H., Vecheri, G. (Eds.), Durability of polymer based composite systems for structural applications, Proceedings of the International Colloquium, 23–27 August 1990, Brussels, Belgium.
- Al-Ostaz, A., Jasiuk, I., 1996. The influence of interface and arrangement of inclusions on local stresses in composite materials. *Acta Materialia* 45, 4131–4143.
- Babuška, I., Andersson, I., Smith, P.J., Levin, K., 1999. Damage analysis of fiber composites Part I: statistical analysis on fiber scale. *Computer Methods in Applied Mechanics and Engineering* 172, 27–77.
- Bonnet, G., 2007. Effective properties of elastic periodic composite media with fibers. *Journal of the Mechanics and Physics of Solids* 55, 881–899.
- Buryachenko, V.A., 2001. Multiparticulate effective field and related methods in micromechanics of composite materials. *Applied Mechanics Reviews* 54, 1–47.
- Buryachenko, V.A., Kushch, V.I., 2006. Effective transverse elastic moduli of composites at non-dilute concentration of a random field of aligned fibers. *Zeitschrift Für Angewandte Mathematik und Physik (ZAMP)* 57, 491–505.
- Buryachenko, V.A., Pagano, N.J., Kim, R.Y., Spowart, J.E., 2003. Quantitative description and numerical simulation of random microstructures of composites and their effective elastic moduli. *International Journal of Solids and Structures* 40, 47–72.
- Brøndsted, P., Lilholt, H., Andersen, S., 1997. Fatigue damage prediction by measurements of the stiffness degradation in the polymer matrix composites. In: International Conference on Fatigue of Composites Eighth International Spring Meeting, Paris, 3–5 June 1997.
- Bystroem, J., 2003. Influence of the inclusions distribution on the effective properties of heterogeneous media. *Composites: Part B* 34, 587–592.
- Chen, X., Papathanasiou, T.D., 2004. Interface stress distributions in transversely loaded continuous fiber composites: parallel computation in multi-fiber RVEs using the boundary element method. *Composites Science and Technology* 64, 1101–1114.
- Cohen, I., Bergman, D.J., 2003. Effective elastic properties of periodic composite medium. *Journal of the Mechanics and Physics of Solids* 51, 1433–1457.
- Crouch, S.L., Mogilevskaya, S.G., 2006. Loosening of elastic inclusions. *International Journal of Solids and Structures* 43, 1638–1668.
- Degrieck, J., Van Paeppegem, W., 2001. Fatigue damage modelling of fibre-reinforced composite materials: review. *Applied Mechanics Reviews* 54, 279–300.
- Dong, C.Y., 2006. Effective elastic properties of doubly periodic array of inclusions of various shapes by the boundary element method. *International Journal for Solids and Structures* 43, 7919–7938.
- Drago, A., Pindera, M.J., 2007. Micro-mechanical analysis of heterogeneous materials: macroscopically homogeneous vs periodic microstructures. *Composite Sciences and Technology* 67, 1243–1263.
- Drugan, W.J., Willis, J.R., 1996. A micromechanics-based nonlocal constitutive equation and estimates of representative volume element size for elastic composites. *Journal of the Mechanics and Physics of Solids* 44, 497–524.
- Eischen, J.W., Torquato, S., 1993. Determining elastic behavior of composites by the boundary element method. *Journal of Applied Physics* 74, 159–170.
- Frayssé, V., Giraud, L., Gratton S., 1998. A Set of Flexible-GMRES Routines for Real and Complex Arithmetics. CERFACS Technical Report TR/PA/98/20.
- Fu, Y., Klimowski, K.J., Rodin, G.J., et al., 1998. A fast solution method for three-dimensional many-particle problems of linear elasticity. *International Journal for Numerical Methods in Engineering* 42, 1215–1229.
- Gamstedt, E.K., Andersen, S.I., 2001. Fatigue Degradation and Failure of Rotating Composite Structures – Materials Characterisation and Underlying Mechanisms. Risø National Laboratory, Roskilde, Denmark.

- Golovchan, V.T., Guz, A.N., Kohanenko, Yu., Kushch, V.I., 1993. Mechanics of composites (in 12 volumes), vol. 1. Statics of Materials. Naukova dumka, Kiev.
- Gorbatkikh, L., Lomov, S., Verpoest, I., 2005. Elastic compliance of a partially debonded circular inhomogeneity. *International Journal of Fracture* 131, 211–229.
- Greengard, L., 1994. Fast algorithms for classical physics. *Science* 265, 909–914.
- Guedes, J.M., Kikuchi, N., 1990. Preprocessing and postprocessing for materials based on the homogenization method with adaptive finite element method. *Computer Methods in Applied Mechanics and Engineering* 83, 143–198.
- Gumbel, E.J., 1958. *Statistics of Extremes*. Columbia University Press, New York.
- Gusev, A.A., 1997. Representative volume element size for elastic composites: a numerical study. *Journal of the Mechanics and Physics of Solids* 45, 1449–1459.
- Hassini, B., Hinton, E., 1998. A review of homogenization and topology optimization I-homogenization theory for media with periodic structure. *Computers and Structures* 69, 707–717.
- Helsing, J., 1995. An integral equation method for elastostatics of periodic composites. *Journal of the Mechanics and Physics of Solids* 43, 815–828.
- Hu, N., Wang, B., Tan, G.W., Yao, Z.H., Yuan, W.F., 2000. Effective elastic properties of 2-D solids with circular holes: numerical simulations. *Composite Sciences and Technology* 60, 1811–1823.
- Joffe, R., 1999. Damage accumulation and stiffness degradation in composite laminates. PhD thesis, Lulea University of Technology, Lulea, Sweden.
- Kantorovich, L.V., Krylov, V.I., 1964. *Approximate Methods of Higher Analysis*. Wiley, New York.
- Kaminski, M., 1999. Boundary element method homogenization of the periodic linear elastic composites. *Engineering Analysis with Boundary Elements* 23, 815–823.
- Kushch, V.I., 1997. Microstresses and effective elastic moduli of a solid reinforced by periodically distributed spheroidal inclusions. *International Journal of Solids and Structures* 34, 1353–1366.
- Kushch, V.I., Shmegeera, S.V., Buryachenko, V.A., 2005. Interacting elliptic inclusions by the method of complex potentials. *International Journal of Solids and Structures* 42, 5491–5512.
- Kushch, V.I., Sangani, A.S., Spelt, P.D.M., Koch, D.L., 2002. Finite Weber number motion of bubbles through a nearly inviscid liquid. *Journal of Fluid Mechanics* 460, 241–280.
- Linkov, A.M., Koshelev, V.F., 1999. Complex variables BIE and BEM for a plane doubly periodic system of flaws. *Journal of the Chinese Institute of Engineers* 22, 709–720.
- Linkov, A.M., 2002. *Boundary Integral Equations in Elasticity Theory*. Kluwer, Dordrecht, Boston.
- Meraghni, F., Blakemad, C.J., Benzeggagh, M.L., 1996. Effect of interfacial decohesion on stiffness reduction in a random discontinuous-fibre composite containing matrix microcracks. *Composites Science and Technology* 56, 541–555.
- Meraghni, F., Desrumaux, F., Benzeggagh, M.L., 2002. Implementation of a constitutive micromechanical model for damage analysis in glass mat reinforced composite structures. *Composites Science and Technology* 62, 2087–2097.
- Mishnaevsky Jr., L., 2007. *Computational Mesomechanics of Composite Materials*. Wiley.
- Mogilevskaya, S.G., Crouch, S.L., 2001. A Galerkin boundary integral method for multiple circular elastic inclusions. *International Journal for Numerical Methods in Engineering* 52, 1069–1106.
- Mogilevskaya, S.G., Crouch, S.L., 2002. A Galerkin boundary integral method for multiple circular elastic inclusions with homogeneously imperfect interfaces. *International Journal for Solids and Structures* 39, 4723–4746.
- Mogilevskaya, S.G., Crouch, S.L., 2004. A Galerkin boundary integral method for multiple circular elastic inclusions with uniform interphase layers. *International Journal for Solids and Structures* 41, 1285–1311.
- Muskhelishvili, N.I., 1953. Some basic problems of the mathematical theory of elasticity. Groningen, P. Noordhoff.
- Paris, F., Correa, E., Mantič, V., 2007. Kinking of transversal interface cracks between fiber and matrix. *Journal of Applied Mechanics* 74, 703–716.
- Prasad, P.B.N., Simha, K.R.Y., 2003. Interface crack around circular inclusion: SIF, kinking, debonding energetics. *Engineering Fracture Mechanics* 70, 285–307.
- Ruggieri, C., Minami, F., Toyoda, M., 1995. A statistical approach for fracture of brittle materials based on the chain-of-bundles model. *Journal of Applied Mechanics* 62, 320–328.
- Saad, Y., Schultz, M.H., 1986. GMRES: a generalized minimal residual algorithm for solving nonsymmetric linear systems. *SIAM Journal on Scientific and Statistical Computing* 7, 856–869.
- Sangani, A.S., Mo, G., 1996. An  $O(N)$  algorithm for Stokes and Laplace interactions of particles. *Physics of Fluids* 8, 1990–2009.
- Sangani, A.S., Yao, C., 1988. Bulk thermal conductivity of composites with spherical inclusions. *Journal of Applied Physics* 63, 1334–1341.
- Shen, H., Brinson, L.C., 2006. A numerical investigation of the effect of boundary conditions and representative volume element size for porous titanium. *Journal of Mechanics of Materials and Structures* 1, 1179–1204.
- Shokrieh, M.M., Lessard, L.B., 2000. Progressive fatigue damage modeling of composite materials. Part I: modeling. *Journal of Composite Materials* 34 (13), 1056–1080.
- Talreja, R., 2000. Fatigue damage evolution in composites – a new way forward in modeling. In: *Proceedings of the Second International Conference on Fatigue of Composites*. 4–7 June 2000, Williamsburg.
- Torquato, S., 2002. *Random Heterogeneous Materials: Microstructure and Macroscopic Properties*. Springer-Verlag, New York.
- Truskett, T.M., Torquato, S., Sastry, S., Debenedetti, P.G., Stillinger, F.H., 1998. Structural precursor to freezing in the hard-disk and hard-sphere systems. *Physical Review E* 58 (#3), 3083–3088.

- Tsai, S.W., 1988. *Composites Design*, fourth ed., Think Composites, Dayton, Ohio.
- Wang, J., Mogilevskaya, S.G., Crouch, S.L., 2005a. An embedding method for modeling micromechanical behavior and macroscopic properties of composite materials. *International Journal of Solids and Structures* 42, 4588–4612.
- Wang, J., Crouch, S.L., Mogilevskaya, S.G., 2005b. A fast and accurate algorithm for a Galerkin boundary integral method. *Computational Mechanics* 37, 96–109.
- Wang, J., Crouch, S.L., Mogilevskaya, S.G., 2006. Numerical modeling of the elastic behavior of fiber-reinforced composites with radially graded interphases. *Composite Sciences and Technology* 66, 1–18.
- Zheng, S.F., Denda, M., Weng, G.J., 2003. Overall elastic and elastoplastic behavior of a partially debonded fibre-reinforced composite. *Journal of Composite Materials* 37, 741–758.